International Journal of Environmental Science and Technology
https://doi.org/10.1007/s13762-021-03767-4

ORIGINAL PAPER

Summer variability in bio-optical properties and phytoplankton pigment signatures in two adjacent high Arctic fjords, Svalbard

S. C. Tripathy[1] · **T. Varunan**[2] · **P. Shanmugam**[2] · **A. U. Kerkar**[1] · **J. T. Bhaskar**[1] · **S. Kurian**[3] · **B. V. Parli**[1] · **M. Gauns**[3]

Received: 25 June 2021 / Revised: 7 September 2021 / Accepted: 26 October 2021

Abstract

Fjords in Svalbard are sensitive to the enhanced climate warming-induced glacial meltwater discharge (fresher, nutrient-rich, turbid) that influences its hydrography and biological processes. This study attempts to explain the impacts of underwater light environment and nutrient limitation on the phytoplankton biomass, composition, and light absorption in the sunlit zone of the Kongsfjorden (KG)–Krossfjorden (KR) twin fjord ecosystem during summer when the meltwater discharge is at maximum. Observations conducted in two phases in each fjord revealed pronounced spatial hydrographic variations between the phases and among the fjords. Intrusion of warm Atlantic water into both fjords and occurrence of subsurface chlorophyll maxima were observed. Meltwater-induced higher concentrations of optically active constituents in KG resulted in a comparatively shallow euphotic zone than KR. Nitrate and silicate limitation ($N/P < 5$, $N/Si > 1$, $Si/P < 3$) was evident in both fjords. Higher phytoplankton light absorption coefficient (a_{ph}, m^{-1}) and chlorophyll-a in KR implied its higher productivity potential. However, the light absorption efficiency of microplankton (at surface) was affected by pigment package effect. Phytoplankton pigments analyses revealed an inter-fjord difference in surface phytoplankton composition predominated by microphytoplankton (49–100%) followed by pico- (0-38%) and nanoplankton (0–18%). The average diversity index for phytoplankton group (H') was higher in KR (0.71) than KG (0.55), which was possibly controlled by microzooplankton grazing. This study reveals that environmental settings in both fjords were quite different, which drives their productivity potential and species diversity. Thus, increased warming climate can have different levels of impacts on fjord ecosystems despite their close geographical proximity.

Keywords Arctic fjords · Bio-optics · Glacial meltwater · Light attenuation · Nutrient limitation · Phytoplankton

Introduction

Global warming affects all regions of the world. However, for their temperature sensitiveness, the Arctic fjords act as indicators of the continuously warming global climate (Cohen et al. 2014). The warming climate is changing the Arctic oceanic ecosystems progressively to a more temperate condition (Vihtakari et al. 2018) known as "Atlantification." Being located at the interface of Arctic and Atlantic oceanic regimes, the Kongsfjorden–Krossfjorden ecosystem undergoes fluctuations in physicochemical variability. Climate change is expected to influence this fjord ecosystem from two directions, i.e., the mouth (opening out into the sea) and the glacial end, where changes in melting of glaciers would influence the physicochemical properties of the fjords (Svendsen et al. 2002). It hence is an ideal fjord system for studying warming-induced changes in the Arctic (Bischof et al. 2019). These high Arctic fjords are influenced by the warm West Spitsbergen Current (WSC) carrying saline Atlantic water (AW) and the coastal current that brings in Arctic water, which is cold and less saline in nature (Vihtakari et al. 2018). An amplified inflow of warm AW displacing the cool Arctic water has accelerated

---

Editorial responsibility: Samareh Mirkia.

S. C. Tripathy
sarat@ncpor.res.in

[1] National Centre for Polar and Ocean Research (NCPOR), Ministry of Earth Sciences, Vasco-da-Gama, Goa 403804, India

[2] Ocean Optics and Imaging Laboratory, Department of Ocean Engineering, Indian Institute of Technology Madras, Chennai 600036, India

[3] CSIR-National Institute of Oceanography, Dona Paula, Goa 403004, India

melting of the tidewater glaciers that terminates straight into the sea (Blaszczyk et al. 2009; Walczowski et al. 2017). The glacial meltwater discharge normally begins in June and ends around September, with a peak during (summer) July–August (Darlington 2015). The meltwater runoff coupled with sediment load and a large amount of mineral particles creates a strong freshwater and turbidity gradient in the water column from inner to outer fjords (Svendsen et al. 2002; Pavlov et al. 2019). The simultaneous intrusion of AW from the outer fjord and fresh, turbid water runoff from the glacial end generates sharp horizontal gradients in the thermohaline and the underwater light environment (reduced thickness of the euphotic layer) along the fjords. This impacts phytoplankton assemblages and affects the growth condition of the phytoplankton (Piquet et al. 2014; van de Poll et al. 2016, 2018; Calleja et al. 2017; Hegseth et al. 2019) that serves as the basis of the marine food web.

Earlier work has shown significant differences in phytoplankton community and production between the geographically closely placed fjords of Spitsbergen that are influenced by the same water masses (Eilertsen et al. 1989). Extensive studies involving hydrography, nutrients, phytoplankton assemblages, and/or optical parameters in Kongsfjorden have been carried out for many years (Svendsen et al. 2002; Hop et al. 2002, 2006; Piwosz et al. 2009; Hodal et al. 2012; Pavlov et al. 2014; Kulk et al. 2018; van de Poll et al. 2018; Halbach et al. 2019; Payne and Roesler 2019) and it is acting as a hot spot for research activities in the Arctic (Bischof et al. 2019) region. However, this cannot be said about the neighboring Krossfjorden, which has geological similarities with the Kongsfjorden. There are few observations concerning phytoplankton assemblages, light regime, nutrients in relation to meltwater, and hydrography in Krossfjorden (Piquet et al. 2014). Moreover, a comparative account of physicochemical and biological parameters between Kongsfjorden and Krossfjorden (Svendsen et al. 2002; Piquet et al. 2010, 2014; Singh and Krishnan 2019) is rare.

This study compared phytoplankton pigments, inorganic nutrients limitation, light absorption coefficients, and hydrography in the two fjords of West Spitsbergen that are greatly influenced by the warm AW and experience rapid glacial melting. The study was carried during summer (August 2016), when the glacial runoff is expected to be maximum (Darlington 2015). Very little is documented pertaining to the possible alteration that might occur in the bio-optical properties and phytoplankton pigment signatures as a consequence of increased "Atlantification." To the best of knowledge, such comparative studies, including the above-mentioned parameters, have not been performed for these fjords. Moreover, the variability in underwater light characteristics and its ecological consequences were investigated in this study. This study hypothesizes that environmental settings influence phytoplankton assemblages (size class, diversity), photosynthetic (light absorption) efficiency, and biomass along and between the fjords through reduced underwater light intensities caused by elevated suspended matter load near the glacial end. This study would further improve existing understandings of the factors that control variability in phytoplankton biomass, composition (diversity), and light absorption efficiency in these two closely located fjords during summer. Furthermore, it is expected that the sea-truth observations of inherent optical properties (IOP) undertaken in this study can possibly be assimilated into radiative transfer and coupled bio-physical models to better explore the underwater light field during summer in these fjords (Cohen et al. 2015; Pavlov et al. 2019) as well as in fjords of similar environmental settings.

Materials and methods

Study site, sampling, and hydrography

The Kongsfjorden–Krossfjorden is a dynamic glacial fjord ecosystem in the high Arctic situated between 78° 40'-77° 30'N and 11° 3'-13° 6'E on the west coast of Spitsbergen in the Svalbard archipelago. The Kongsfjorden (KG) is oriented from southeast to northwest, while Krossfjorden (KR) is oriented from north to south. KG is 20 km in length, and its width varying from 4–10 km, whereas KR is 30 km long, its width varying between 3 and 6 km. This double fjord ecosystem shares a common mouth located at 79°N and 11°E, and is influenced by the freshwater discharge from surrounding glaciers, which is minimal in winter and maximum during the summer season (Svendsen et al. 2002). The intrusion of relatively warm water brought in by the west Spitsbergen current (WSC) at irregular intervals changes the water mass within these fjords from Arctic predominance during winter to Atlantic predominance during summer season (Svendsen et al. 2002), thereby strongly influencing the physicochemical and biological properties of the ecosystem inside the fjords (Hop et al. 2002).

For this study, ten stations were sampled along the fjords allowing a comparison of variables in the meltwater gradient. Five stations in Kongsfjorden (KG1, KG2, KG3, KG4, KG5), four in Krossfjorden (KR1, KR2, KR3, KR4), and one in the open ocean (O1) are located in the common mouth region (Fig. 1). Water sampling and profiling of radiometer was carried out onboard research boat *MS-Teisten*. Water samples were collected from three depths (0, 30, 60 m) using 10 L Niskin samplers. The overall depth along the sampling transects ranges from < 50 m near the glacial end to > 300 m near the mouth. To study the short-term temporal variation along these dynamic fjords, sampling was carried out in two phases, i.e., phase-1 (2–3 August 2016) and phase-2 (11–12 August 2016) (Table 1).

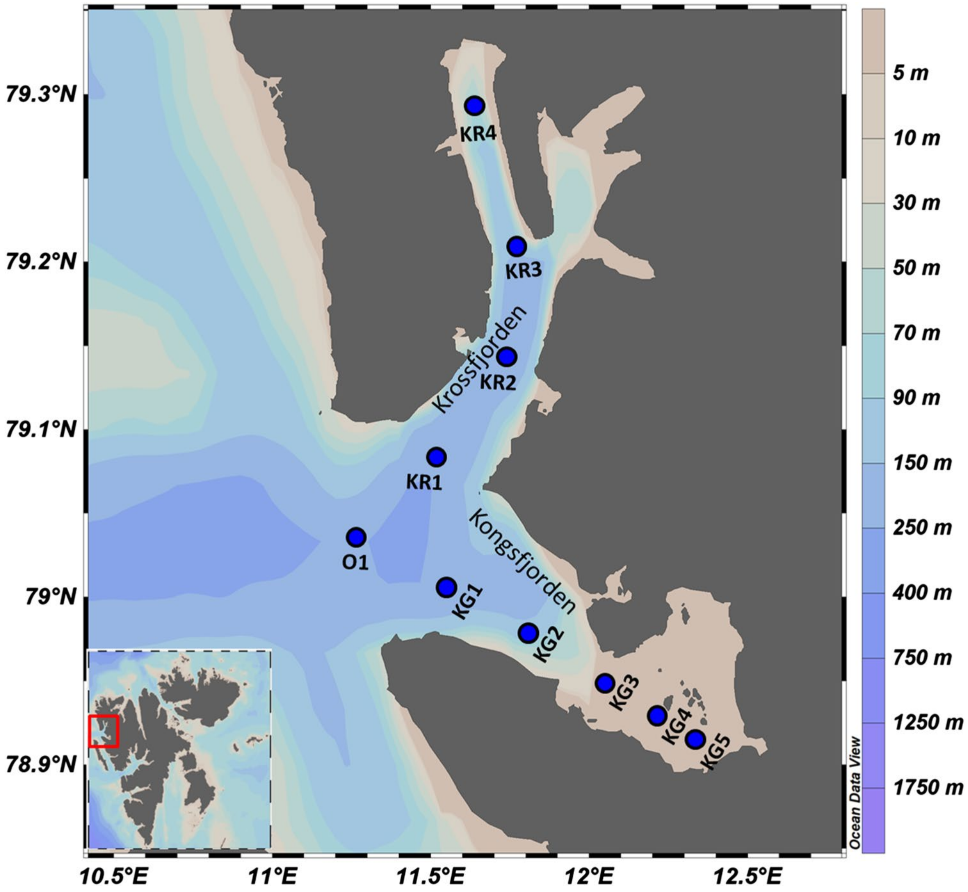

Fig. 1 Map showing the sampling locations (blue closed circles) in Kongsfjorden (KG) and Krossfjorden (KR). Background color indicates the bathymetry (m). The inset figure shows a larger perspective of the study area

Table 1 Sampling details and some of the variables measured in both fjords. Surface PAR values apply to all stations of the respective fjords

Parameters	Stations									
	KG5	KG4	KG3	KG2	KG1	O1	KR4	KR3	KR2	KR1
Lat. (°N)	78.89	78.90	78.94	78.95	79.01	79.03	79.25	79.21	79.11	79.06
Long. (°E)	12.32	12.22	12.14	11.82	11.60	11.28	11.70	11.86	11.75	11.50
Phase-1 [02–03 August 2016]										
SST (°C)	5.3	5.5	6.1	4.4	–	6.4	3.3	2.3	6.0	6.2
$\mathrm{Chl_{int}}$ (mg $\mathrm{m^{-2}}$)	8.98	14.53	0.78	8.91	–	4.74	3.16	12.73	8.09	2.13
Avg. TSM (mg $\mathrm{l^{-1}}$)	14.41	12.91	10.83	12.22	–	15.13	15.06	14.65	14.3	14.35
Surface PAR (μmol $\mathrm{m^{-2}\ s^{-1}}$)	749					771				
$\mathrm{K_d}$ ($\mathrm{m^{-1}}$)	0.56	0.91	0.41	0.25	–	0.14	0.33	0.22	0.31	0.34
$\mathrm{Z_{eu}}$ (m)	12.31	7.52	16.68	26.86	–	49.13	20.79	30.15	21.63	19.84
Phase-2 [11–12 August 2016]										
SST (°C)	4.5	4.5	4.5	5.1	5.5	5.5	5.1	5.7	4.3	4.8
$\mathrm{Chl_{int}}$ (mg $\mathrm{m^{-2}}$)	5.21	2.97	1.91	2.65	17.18	9.62	38.05	6.29	5.98	3.55
Avg. TSM (mg $\mathrm{l^{-1}}$)	13.6	10.16	11.0	10.79	12.0	10.37	15.31	12.76	12.29	10.33
Surface PAR (μmol $\mathrm{m^{-2}\ s^{-1}}$)	470					241				
$\mathrm{K_d}$ ($\mathrm{m^{-1}}$)	0.71	0.50	0.42	0.12	0.15	0.11	0.21	0.21	0.33	0.25
$\mathrm{Z_{eu}}$ (m)	9.61	13.56	16.06	56.13	44.86	61.82	32.40	32.51	20.87	27.60

*Avg. (average) indicates mean value of the three depths

A hyperspectral radiometer (HyperPro II, Satlantic, Canada) was deployed in free-fall profiling mode to record hydrography in the euphotic zone (Z_{eu}; described as the depth interval down to 0.1% light). Vertical profiles of temperature (°C) and salinity were measured by CTD probe integrated with profiling radiometer body. Photosynthetically active radiation (PAR, μmol m^{-2} s^{-1}) was measured by the inbuilt irradiance sensors. Chl-*a* fluorescence, colored dissolved organic matter (CDOM, in ppb), and turbidity (NTU at 700 nm) were measured by the free-fall profiling (vertical velocity: ~ 0.3 m s^{-1}) of a hyperspectral radiometer equipped with ECO triplet pack (WET Labs®). While deploying the radiometer, care was taken to avoid ship shade and ship-induced disturbances/vibrations. The obtained radiometric measurements (with $< 5°$ tilt) were processed by ProSoft software, and downward cast data were considered for interpretation. Downwelling diffused irradiance attenuation coefficient (K_d, m^{-1}) was derived by linear regression fitting of log-transformed PAR data. The Z_{eu} was calculated as: $Z_{eu}(m) = -\ln(0.001)/K_d$. Sea surface temperature (SST) was measured using a bucket thermometer (Theodor Friedrichs & Co, Germany) with a measurement accuracy of ± 0.2 °C.

Phytoplankton pigments and macronutrients

Total phytoplankton biomass or chlorophyll-*a* (Chl-*a*) was quantified by filtering 3 l of water samples onto 47 mm GF/F filters (Whatman®) under low suction pressure in dim light conditions followed by overnight extraction of the filters with 10 ml of AR grade 90% acetone at 4 °C. The extracts were then measured fluorometrically (10-AU, Turner® Designs) before and after the addition of 10% HCl to quantify Chl-*a* and phaeopigments (degraded phytoplankton pigments) concentrations (JGOFS 1994). The ratio Chl-*a*/phaeopigments (Pheo) is often used as a proxy for phytoplankton cell degradation products generated by zooplankton grazing (because herbivores convert Chl-*a* to Pheo) and/or cell senescence under reduced environmental growth conditions (Welschmeyer and Lorenzen 1985). The entire assay was carried out in dim light or dark to avoid photo-degradation of phytoplankton pigments. The Chl-*a* concentrations (mg m^{-3}) at different depths were trapezoidally integrated to estimate the water column Chl-*a* value (mg m^{-2}) at each sampling location.

For analysis of other phytoplankton pigments, 3 l of seawater was filtered onto GF/F filters (0.7 µm, 25 mm, Whatman®) in a dark and cold room, and the pigments were stored at − 80 °C until further analysis. For logistical limitation, samples for high-performance liquid chromatography (HPLC) analysis were collected for phase-1 only. The preserved filters were soaked in 100% methanol for extraction of pigments and subsequently analyzed by a HPLC (Agilent Technologies) equipped with an Eclipse XDB C8 column. The pigments were segregated by a dual solvent gradient (solvent A: methanol (70%)/0.5 M ammonium acetate (30%); solvent B-100% methanol) as detailed in Kurian et al. (2012). The marker pigments were selected in reference to the phytoplankton groups observed in previous studies in the Kongsfjorden (Bhaskar et al. 2016; van de Poll et al. 2016) and Svalbard (Pettersen et al. 2011) regions. For phytoplankton taxa classification, the diagnostic pigments (DP) were taken as the sum of seven pigments (Supplementary Table 1B) such as fucoxanthin, peridinin, alloxanthin, 19′-hexanoyloxyfucoxanthin (19′HF), 19′-butanoyloxyfucoxanthin (19′BF), zeaxanthin, and TChl-b (Chl-b + divinyl chlorophyll-b (DivChl-b)) according to Uitz et al. (2006). The biomass proportion for different size classes such as picoplankton (< 2 µm), nanoplankton (> 2 and < 20 µm), and microplankton (> 20 and < 200 µm) was differentiated based on the ratio of the different pigments to DP (Supplementary Table 1C). However, Uitz et al. (2006) is a global model but has been successfully used in many varied geographical locations, including high latitudes (the Arctic and the Southern Ocean). Despite the fact that DP-based indices have some limitations, they are still widely used to study the composition of phytoplankton communities with contributions from different cell sizes (micro-, nano-, and pico-phytoplankton). Thus, using DP, the size-fractioned contributions of phytoplankton (f_{micro}, f_{nano}, and f_{pico}) were derived as follows:

$$f_{\text{micro}}\% = 100 \times \left(1.41\,[\text{fucoxanthin}] + 1.41\left[\text{peridinin}\right]\right) / \Sigma\text{DP}\ (> 20\ \mu m) \tag{1}$$

$$f_{\text{nano}}\% = 100 \times (0.60\,[\text{alloxanthin}] + 0.35[19\prime\text{BF}] + 1.27[19\prime\text{HF}]) / \Sigma\text{DP}\ (2\ \text{to}\ 20\ \mu m) \tag{2}$$

$$f_{\text{pico}}\% = 100 \times (0.86\,[\text{zeaxanthin}] + 1.01[\text{TChlb}]) / \Sigma\text{DP}\ (< 2\mu\text{m}) \tag{3}$$

Shannon Weaver index for phytoplankton group diversity (H') was calculated according to Shannon and Weaver (1949), whereas group evenness (J') was derived as ($J' = H'/\log_2 G$) as suggested by (Pielou 1966). Evenness index is the ratio of observed diversity to highest diversity, and it is attained when most groups in a sample are equally abundant.

An aliquot (100 ml) of water samples was collected directly from the Niskin sampler into acid cleaned plastic bottles and was stored at − 20 °C until used for estimating concentrations (µM) of nitrate ($NO_3^- + NO_2^-$), nitrite (NO_2^-), phosphate (PO_4^{3-}), and silicate (SiO_4^{4-}) by a continuous flow autoanalyzer (Model AA3, Seal Analytical Ltd., GmbH, Germany) adopting standard colorimetric methods (JGOFS 1994). Calibration was carried out using potassium nitrate, sodium nitrate, sodium meta-silicate, and potassium hydrogen phosphate standards for analyses of NO_3^-, NO_2^-, SiO_4^{4-}, and PO_4^{3-}, respectively. The standard error of $<2\%$ was set for all triplicate analyses of nutrient samples. The precision of detection (limits) for NO_3^-, PO_4^{3-}, and SiO_4^{4-} were ±0.06 (±0.07), ±0.003 (±0.004), and ±0.06 (±0.04) µM, respectively.

Light absorption coefficients and suspended matter

The water samples collected from discrete depths by the Niskin sampler were analyzed for measuring light absorption coefficients of phytoplankton and detritus through QFT (quantitative filter technique) suggested by Mitchell (1990). One to two liter of sample from each depth was filtered separately onto a GF/F filter (0.7 µm, 25 mm) under a maintained low suction pressure. Subsequently, the filters were measured within 400–700 nm wavelength at 1 nm interval using a double-beam UV–VIS spectrophotometer (UV-2600, Shimadzu Corp., Japan) equipped with an integrating sphere. A GF/F filter paper soaked with freshly prepared filtered seawater (FSW) was used as a reference while carrying out these measurements. The path-length amplification effect of the glass fiber filter caused due to multiple scattering was corrected according to Cleveland and Weidemann (1993):

$$\mathrm{OD_s}(\lambda) = 0.378\,\mathrm{OD_f}(\lambda) + 0.523\,\mathrm{OD_f}(\lambda)^2 \tag{4}$$

where $\mathrm{OD_s}(\lambda)$ and $\mathrm{OD_f}(\lambda)$ are optical density (OD) of the particulate matter in suspension and filter, respectively. The clearance area of each filter paper was measured thrice using a digital Vernier caliper, and an average of the three was taken as the measure for clearance area. Further, the light absorption coefficient of the total particles ($a_p(\lambda)$) present in the suspension was calculated as follows:

$$a_p(\lambda) = 2.303\,\mathrm{OD_s}(\lambda) * S/V \tag{5}$$

where 2.303 = conversion factor for $\log_{10}$ to $\log_e$, S = clearance area measured for the filter paper (m^2), V = filtered volume (m^3), and S/V = approximate geometrical light pass length.

Subsequently, the filter papers were soaked in a 2% solution of calcium hypochlorite ($Ca(ClO)_2$) for 20 min to bleach the algal pigments (Woźniak et al. 1999). After rinsing with FSW, the absorbance of the decolorized papers was re-measured to obtain OD of the non-phytoplankton particles or detritus ($a_d(\lambda)$) using Eq. (5). Phytoplankton light absorption coefficient ($a_{ph}(\lambda)$) was calculated by substituting $a_d(\lambda)$ from $a_p(\lambda)$, and using the $a_{ph}(750)$ value as the null point correction (Mitchell et al. 2002; Stramska et al. 2003). The mean values of duplicate spectra were analyzed in this study. The chlorophyll-specific phytoplankton pigments absorption coefficient ($a^*_{ph}(\lambda)$) for a particular sample was calculated as a ratio of the $a_{ph}(\lambda)$ to Chl-*a* concentration.

The light absorption coefficient for CDOM (a_{CDOM}) was measured by filtering 200 ml of water samples through 47 mm GF/F (®Whatman) to eliminate the larger particles and then filtered through 47 mm membrane filters (Millipore, 0.2 µm) to eliminate the smaller particles. Subsequently, the filtrates were equilibrated to room temperature by storing them in dark conditions. The absorption measurements were carried out spectrophotometrically (UV-2600, Shimadzu, Japan) using quartz cuvettes (path-length: 10 cm) and Milli-Q water as a reference. Absorbance spectra were obtained between 350 and 750 nm at a 1 nm interval. Spectral absorbances were normalized to zero at 600 nm due to temperature-dependent artifacts. The absorption coefficient of CDOM (m^{-1}) was calculated adopting the equation of Mitchell et al. (2002) as given below:

$$a_{\mathrm{CDOM}}(\lambda) = \frac{2.303}{L}\left[\left\{\mathrm{OD_s}(\lambda) - \mathrm{OD_{fsw}}(\lambda)\right\} - \mathrm{OD_{null}}\right] \tag{6}$$

where 2.303, L, $\mathrm{OD_s}$, $\mathrm{OD_{fsw}}$, and $\mathrm{OD_{null}}$ are the conversion factor from $\log_{10}$ to $\log_e$, optical (cuvette) path-length in meters, optical densities of the sample, purified filtered seawater (FSW), and at null absorption wavelength. The spectral slope of CDOM absorption coefficient (S) was derived by nonlinear exponential regression fitting of a_{CDOM} coefficient versus wavelength (350–650 nm) as per the approach of Stedmon et al. (2000). The S is the exponential slope coefficient, which indicates a decrease in absorption with respect to wavelength. The S value varies with the source of the CDOM.

For estimating total suspended matter (TSM in mg l^{-1}), 2 l of water samples was filtered through pre-burned (at 60 °C for 4 h) and pre-weighed (w_1 in mg) 47 mm millipore filters (pore size 0.45 µm) under maintained low vacuum pressure (approx. 120 mm Hg); then, the filters were oven-dried at 60 °C for 4 h and re-weighed to obtain the final weight (w_2 in mg). The concentration of TSM was obtained by subtracting w_1 from w_2 (JGOFS 1994).

Results and discussion

Variability in hydrographical conditions

In Kongsfjorden (phase-1), the vertical temperature varied from 3.75 to 6.34 (avg. 4.83 ± 0.68 °C), whereas salinity varied from 28.92 to 34.96 (34.45 ± 0.93). Cooler and fresher water in inner fjord were observed with a clear thermal front-like feature in the mid fjord. Low salinity water spreads outward, forming a clear halocline (Fig. 2a). In phase-2, temperature ranged between 3.74 and 6.40 (avg. 4.49 ± 0.63 °C), while salinity ranged from 31.48 to 35.03 (34.65 ± 0.55). Though temperature–salinity ranges were similar in both phases, intrusion of warmer water to inner

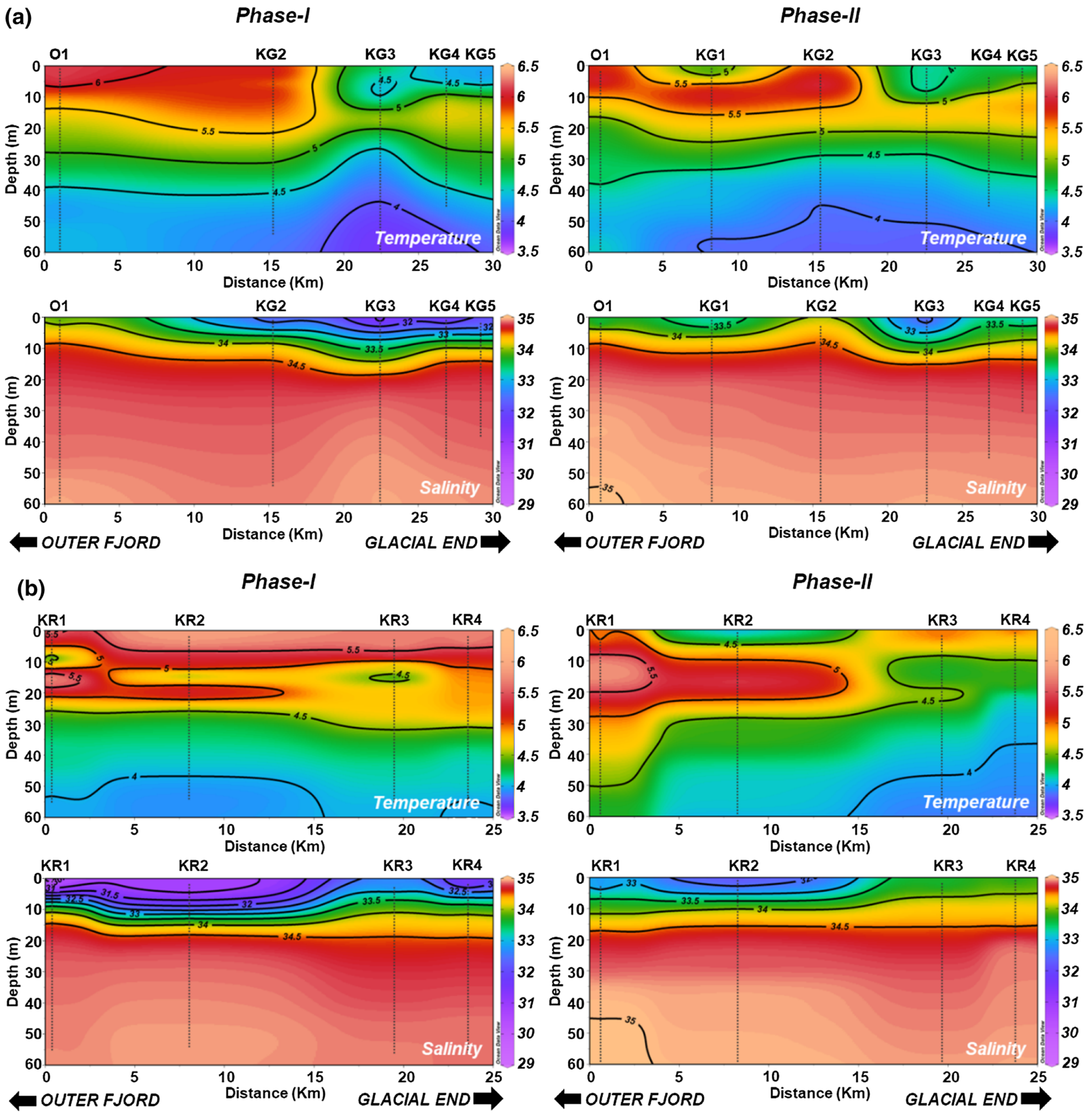

Fig. 2 Vertical distribution diagrams of temperature (top panels) and salinity (bottom panels) during both the phases in (**a**) Kongsfjorden and (**b**) Krossfjorden. The station locations as shown in this figure are also applicable to all other distribution diagrams

fjord was discernible, and shoaling of salinity contours in the mid fjord was observed, indicating wind and/or tide-induced mixing (Fig. 2a). The presence of less freshwater in the upper 10 m at the glacial end indicated probably lessened melting in phase-2 or the presence of intruded warmer water.

In Krossfjorden (phase-1), water column temperature ranged from 3.11 to 6.00 (avg. 4.50 ± 0.58 °C), as salinity ranged between 30.03 and 34.92 (avg. 34.28 ± 1.08). Unlike Kongsfjorden, a more uniform distribution of temperature and salinity was observed in the upper 10 m with lesser gradients. A salinity difference of nearly 2 was observed between the inner and outer fjord (Fig. 2b). In phase-2, temperature varied from 3.12 to 5.97 (avg. 4.41 ± 0.54 °C), while salinity varied from 32.03 to 35.05 (avg. 34.63 ± 0.53). A tongue-like structure from the outer fjord was sandwiched between cooler water from subsurface and meltwater discharge from *Julibreen* glacier (near to station KR2), which significantly influenced the fjord water and resulted in unconventional lower salinity at the mouth than the glacial end region. Relatively higher salinity at the glacial end (Fig. 2b) implied less melting and/or uplifting of more saline outer subsurface water in the inner fjord.

Both fjords were observed to be influenced by Atlantic-origin warm, and saline water (AW) masses superimposed by a slim layer of fresh and cool surface water (SW) runoff from the glaciers. Both the water masses variations were within the historically reported range, and stratification was driven by salinity than temperature. Payne and Roesler (2019) have also observed distinctive surface water (SW: $T = 1$–5 °C, $S < 34.7$, 0–15 m) and AW ($T = 5.5$–7 °C, $S > 34.9$, 15–60 m) in the Kongsfjorden during summer (August 2014), which was found to be significantly higher than the historical observations. Stratification of similar nature has been reported every year in the fjords of Svalbard (Eilertsen et al. 1989; Piwosz et al. 2009; Singh and Krishnan 2019); however, the amount of AW in the fjords is often modulated by the prevailing oceanographic conditions in the North Atlantic (Cottier et al. 2005). Irrespective of proximity to the glacial end, where high discharge of freshwater occurs, stratification was observed throughout the fjord with occasional shoaling of thermohaline contours (phase-2) in the mid fjord, indicating upward movement of the water masses probably caused by wind flow or bottom topography in Kongsfjorden. The stratification in Krossfjorden was strongly influenced by the meltwater from the *Julibreen* glacier situated near the outer fjord, where the drop in salinity was noticed, but the temperature range was maintained, showing increased values in the surface water (Fig. 2b phase-1). The difference in the intrusion of AW into the fjords and/or strength of glacial melting could be clearly discerned between the sampling phases indicating the dynamic oceanographic features of both fjords. Comparatively, phase-2 of sampling witnessed less melting and/or more intrusion of AW into both fjords. The amalgamation of inflowing AW and surface freshwater runoff resulted in complex hydrographical features, and increasing stratified conditions (Calleja et al. 2017). The observed stratification in this twin fjord ecosystem signified a shift from the Arctic to Atlantic predominance in summer (Svendsen et al. 2002; David and Krishnan 2017). Previously it is observed that, if the fjord is predominated by cold Arctic water, a distinct hydrographical front develops at the fjord entrance separating the fjord ecosystem from the AW incursion (Svendsen et al. 2002; Cottier et al. 2007), which was not the case during the study period indicating intrusion of AW into the fjords.

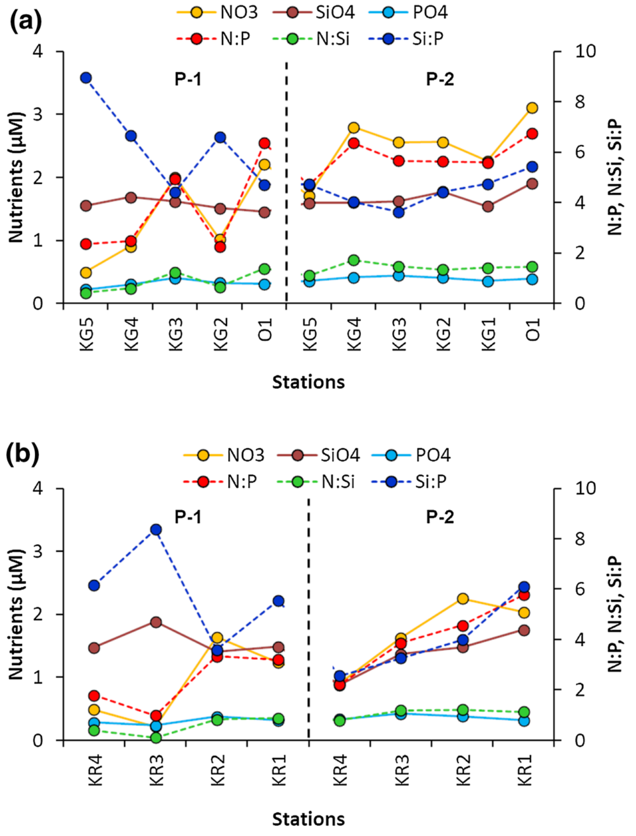

Fig. 3 Mean concentration of macronutrients (NO_3^-, PO_4^{3-}, SiO_4^{4-}) and their ratios (N/P, N/Si, Si/P) in the water column of (**a**) Kongsfjorden and (**b**) Krossfjorden. The dashed vertical line separates the phase-1 (P-1) and phase-2 (P-2) sampling

Macronutrients availability

The macronutrients, i.e., NO_3^-, NO_2^-, PO_4^{3-}, and SiO_4^{4-}, in Kongsfjorden (Fig. 3a) and Krossfjorden (Fig. 3b) were within the ranges of the reported values (Piquet et al. 2014) and showed nearly identical concentrations in both fjords. Not much variation was recorded in PO_4^{3-} and SiO_4^{4-} along the fjord, but NO_3^- availability was more toward the outer fjord compared to the mid and inner fjord as was observed by Calleja et al. (2017).

In Kongsfjorden, the observed mean ratio of $N/P < 5$ and $N/Si \geq 1$ in phase-1 slightly improved in phase-2. Low elemental (N/P and N/Si) ratio implied N- and Si-limited condition throughout the fjord was indicative of conducive environmental settings for growth of non-siliceous phytoplankton such as *Phaeocystis* spp. and heterotrophic/mixotrophic dinoflagellates (Bhaskar et al. 2016, 2020). Earlier, low N/P ratios were reported in summer (Iversen and Seuthe 2011; Seuthe et al. 2011) and during the post-bloom (June) period (van de Poll et al. 2016, 2018), when elevated ammonium concentration than NO_3^- concentration at surface signified shift from new production (NO_3^--based) to regenerated production in Kongsfjorden dominated by diverse flagellated phytoplankton (van de Poll et al. 2016). Nitrogen and Si-limitation were also ubiquitous in Krossfjorden, and it was even more severe. Piquet et al. (2014) observed a similar limiting condition in Krossfjorden. Very low Si/P ratio (< 5) insinuated probable succession of Green algae/cyanobacteria over microplankton (Harrison et al. 1977; Levasseur and Therriault 1987) in this fjord. It has been reported that in summer increase in glacial meltwater input leads to a buildup of ammonium and low concentrations of NO_3^- caused by reduced nitrification during non-bloom circumstances and the utilization of existing NO_3^- (Calleja et al. 2017). However, it still remains unclear about the source, nature, and fate of the biogeochemical materials supplied to the fjord water through enhanced melting of glaciers, which makes it difficult to quantify the impact of various types of meltwater on the nutrient fluxes of these fjord ecosystems (Beaird et al. 2015). Generally, nitrogen is considered as the principal limiting nutrient in the coastal Arctic region (Piquet et al. 2014; van de Poll et al. 2016), as was noticed in the study area, and in the Arctic at large (Popova et al. 2010).

Light attenuation in relation to variability in turbidity and CDOM

The surface PAR variability indicated comparatively less light availability during phase-2 (Table 1), which could be ascribed to the overcast sky conditions. From the downwelling diffused light attenuation coefficient (K_d) values, it could be inferred that relatively clear water column and deeper euphotic depth (Z_{eu}, 1% light depth) prevailed in Krossfjorden than Kongsfjorden (Table 1). Usually, shallower Z_{eu} observed at glacial end deepened toward the mouth region in Kongsfjorden as observed previously (Piquet et al. 2014); nevertheless, Krossfjorden witnessed shallower Z_{eu} toward the outer fjord stations, which could be attributed to impact of meltwater from the nearby (*Julibreen*) glacier that brings in optically active substances (OAS) like turbidity and CDOM.

The interrelationship between K_d and other environmental variables was different among and between the fjords (Table 2). In Kongsfjorden, during phase-1, the K_d showed a moderate positive relationship with CDOM ($R^2 = 0.55$), turbidity ($R^2 = 0.50$), and Chl_{int} ($R^2 = 0.46$); and negative relationship with salinity ($R^2 = 0.49$) signifies that the freshwater generated CDOM and turbidity was more predominant in controlling the K_d in Kongsfjorden as reported earlier (Piwosz et al. 2009; Pavlov et al. 2014; Payne and Roesler 2019; Halbach et al. 2019); whereas, no such associations were observed for Krossfjorden where K_d showed no correlation with CDOM and turbidity but showed a significant negative relationship with Chl_{int} ($R^2 = 0.98$, $p < 0.05$) stronger negative relationship with salinity ($R^2 = 0.57$), implying that variation in K_d was more predominantly influenced by OAS in Kongsfjorden than in Krossfjorden. Previous report has shown that surface water in the inner Krossfjorden is often characterized as less turbid in comparison to waters of inner Kongsfjorden (Piquet et al. 2010). Phase-wise breaks up of data analyses (Table 2) revealed that whenever K_d showed a strong or significant relationship with Chl_{int}, its relationship with CDOM and/or turbidity was weak and vice versa.

Table 2 Linear regression coefficients of determination (R^2) between light attenuation coefficient (K_d) and other oceanographic variables in the study area

Variables	Kongsfjorden		Krossfjorden	
	(P-I)	(P-II)	(P-1)	(P-II)
Salinity	**0.49**	***0.76**	**0.57**	***0.87**
TSM (mg l^{-1})	–	0.27	–	**0.16**
NTU (700 nm)	0.50	*0.92	–	**0.32**
CDOM (ppb)	0.55	*0.94	–	**0.47**
Chl_{int} (mg m^{-2})	0.46	**0.20**	***0.89**	**0.21**

*Significant at $p < 0.05$; values in bold indicate inverse relationship; dash indicates no correlation

In Kongsfjorden, the turbidity and CDOM concentrations were comparatively higher in phase-1 than phase-2 (Fig. 4). Elevated turbidity and CDOM were observed at the inner and mid-fjord stations (KG5, KG4, KG3), which rapidly decreased toward the outer fjord. High turbidity and CDOM in the inner fjord were basically originated from glacial inputs or mixing-induced resuspension of bottom sediments (Halbach et al. 2019). Conversely, in Krossfjorden, both variables were uniformly distributed throughout in the upper 10–15 m during both the phases. Higher values were observed in the outer fjord station (KR2), which could be linked to meltwater from the nearby (*Julibreen*) calving glacier. Turbidity and CDOM showed significant inverse linear relationships with salinity in both fjords (Fig. 5). Significant positive linear relationship (figure not shown) between turbidity and CDOM in Kongsfjorden ($R^2 = 0.95$, $p < 0.001$) and Krossfjorden ($R^2 = 0.82$, $p < 0.001$) indicated their analogous distribution pattern, and probable origin from the same source, i.e., from glacial meltwater.

The presence of CDOM is ubiquitous in all natural waters and is generated from the degradation of plant materials both of terrestrial and aquatic origin (Kirk 1994). It plays a significant role in underwater light attenuation. CDOM spectral slope (S) is a proxy for origin (marine vs. terrestrial) of CDOM, with usually lower slopes for freshwater and coastal waters as compared to the high saline open ocean waters (Stedmon and Markager 2001), which contains marine humic substances and newly formed biological CDOM (Ferrari 2000), and photo-bleached CDOM (Para et al. 2010).

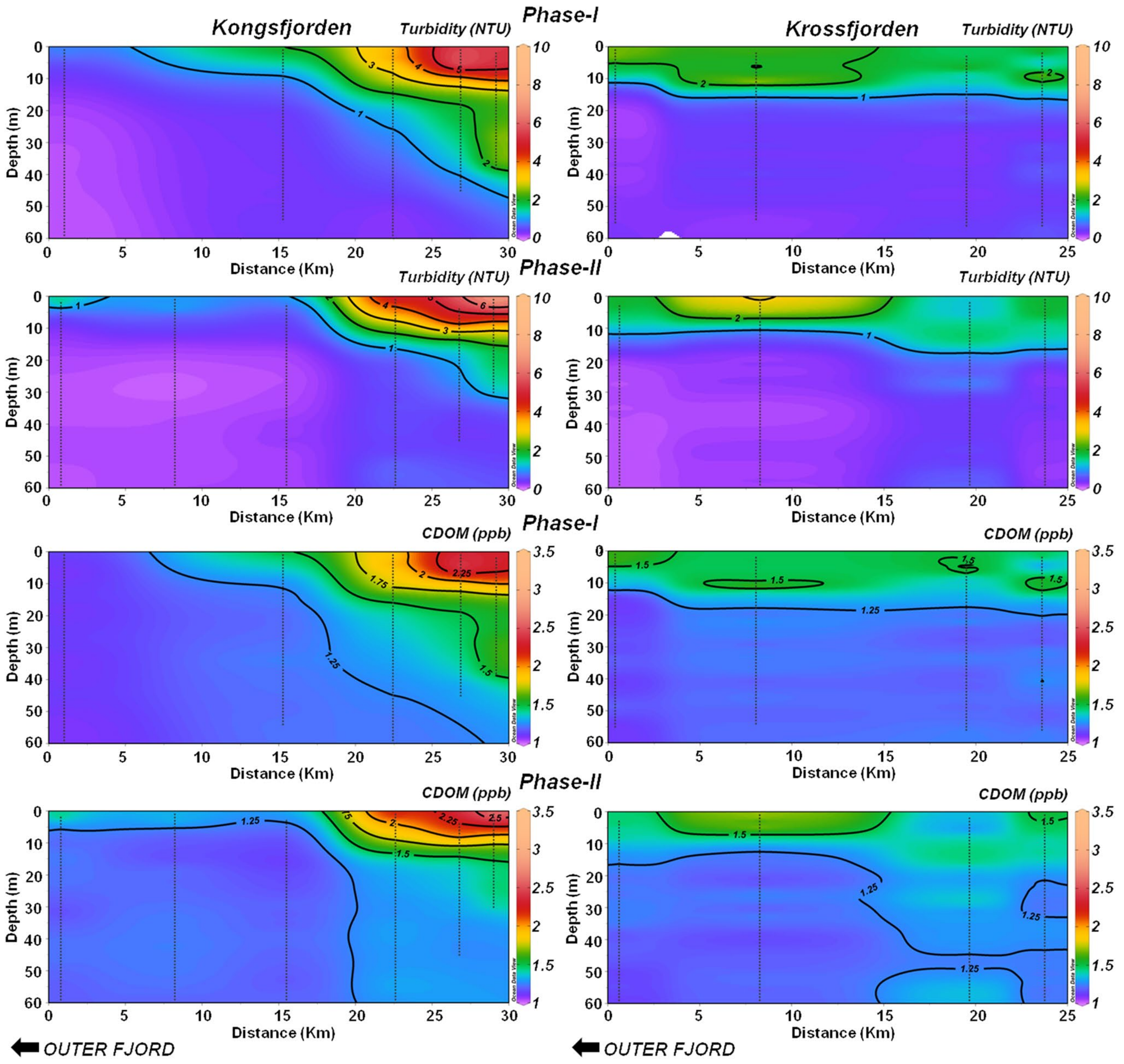

Fig. 4 Depth distribution of turbidity (NTU) and colored dissolved organic matter (CDOM) in the Kongsfjorden (left panels) and Krossfjorden (right panels) during both the phases measured by hyperspectral radiometer equipped with ECO triplet

Hence, to identify the source of CDOM, spectral slope analysis was performed. The mean value of CDOM spectral slope ($S_{350\text{-}650}$) was $0.014 \pm 0.003\ \mathrm{nm}^{-1}$ and $0.011 \pm 0.001\ \mathrm{nm}^{-1}$ in Kongsfjorden and Krossfjorden, respectively, indicating higher S values in the Kongsfjorden. The mean slope for the entire study area was $0.013 \pm 0.003\ \mathrm{nm}^{-1}$, which is consistent with the value of Bricaud et al. (1981), who observed that the S values varied between 0.010 and $0.020\ \mathrm{nm}^{-1}$ (mean $0.014\ \mathrm{nm}^{-1}$) for different oceanic and coastal regions. The S values of surface samples (0 m) were higher toward the outer fjord and showed a weak positive relationship with salinity in Kongsfjorden ($R^2 = 0.27$). Conversely, the values were almost even throughout the fjord and showed an inverse relation with salinity in Krossfjorden ($R^2 = 0.10$). No relationship was observed for subsurface S values and salinity in both fjords.

Autochthonous (produced in situ) CDOM differs from oceanic CDOM by having lower S values (Stedmon et al. 2011). Thus, the lower average S value noticed in Krossfjorden could be ascribed to more of autochthonous in origin (in situ production of organic matter by phytoplankton), whereas the higher S values in Kongsfjorden

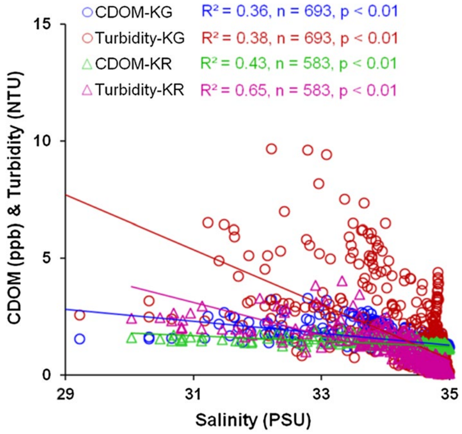

Fig. 5 Scatter plots showing relationship of CDOM and turbidity with salinity in Kongsfjorden and Krossfjorden during both the phases combined

could be due to input of terrestrial organic matter during the ice-melting (Calleja et al. 2017). However, the higher *S* values observed could likely imply mixing of low-intensity autochthonous CDOM (low *S* values) and with oceanic CDOM having higher *S* values (Stedmon et al. 2011; Kowalczuk et al. 2019). Considering the comparatively meager vegetation on Svalbard, the supply of organic matter (as well as CDOM) is low from terrestrial sources (Johansen and Tømmervik 2013), as compared to what was released by large Arctic rivers (Stedmon et al. 2011). The contribution of terrestrially originated CDOM is found to be significant in various coastal environments; however, it is believed to be low in Kongsfjorden, where autochthonous production of CDOM associated with bacterial activities has been documented (Pavlov et al. 2014). Furthermore, Pavlov et al. (2014) have observed the prevalence of marine-originated CDOM in surface waters of the fjord. Thus, the observed *S* values in Kongsfjorden could also be due to the advection of CDOM by AW (Pavlov et al. 2014). The relationship between *S* values and salinity in Kongsfjorden (positive) and Krossfjorden (negative) corroborates this fact. However, studies have emphasized that terrestrial sources of CDOM in Kongsfjorden might be more important than previously believed (Calleja et al. 2017). The observed difference in CDOM concentration between the fjords can affect the light-harvesting efficiency of the thriving phytoplankton. Light absorption by CDOM is highest in the UV range, and it exponentially decreases to zero as wavelength increases (Stedmon and Markager 2001). Change in underwater light spectral quality, in the wavelength range preferred by phytoplankton, can occur due to a small increase in CDOM absorption that would possibly increase the competition between various phytoplankton groups leading to enhanced photo-acclimation, and even reduced growth in some phytoplankton species/group that depends on preferential utilization of light at shorter wavelengths (Pavlov et al. 2014).

Factors influencing phytoplankton biomass, community structure, and diversity

Phytoplankton biomass and phaeopigments

In Kongsfjorden, the fluorometrically measured Chl-*a* and Pheo varied from ND-1.02 (0.17 ± 0.27 mg m^{-3}) and ND-0.64 (0.14 ± 0.19 mg m^{-3}), respectively, while it varied from ND-2.29 (0.21 ± 0.48 mg m^{-3}) and ND-0.72 (0.12 ± 0.18 mg m^{-3}), indicative of relatively higher Chl-*a* and lower Pheo in Krossfjorden. Fluorescence profiles from the radiometer corroborated the fluorometric measurements. In Kongsfjorden, high fluorescence coexisted with cooler water and increased with depth toward outer fjord during phase-1, whereas clear subsurface maximum and reasonably higher fluorescence was observed at mid and outer fjord during phase-2 (Fig. 6). Furthermore, enhancement of surface fluorescence could be linked to shoaling of salinity contours during phase-2. In Krossfjorden, probable less melting from the inner fjord helped the advancement of outer fjord water that brings in more nutrients (Halbach et al. 2019) and thereby augmented fluorescence. Higher subsurface fluorescence (at 10 m) observed in the mid and outer fjord during phase-1 was found to have extended to the surface as well as to the inner fjord in phase-2 (Fig. 6), implying inward movement of waters. Sigma-t (density, Kg m^{-3}–1000) increased with depth (Fig. 1S, supplementary material), indicating that both fjords water column was stable, and the chlorophyll fluorescence observed during this study existed in the most stable water layers in both fjords. The observed higher Chl-*a* fluorescence in the outer fjords compared to the inner fjord is in line with the earlier works (e.g., Hodal et al. 2012; Hegseth and Tverberg 2013; Piquet et al. 2014; Bhaskar et al. 2016; Payne and Roesler 2019) that reported higher phytoplankton biomass and productivity at the outer Kongsfjorden compared to the inner region. In general, higher fluorescence was observed in phase-2 in both fjords, which was also reflected in column integrated Chl-*a* (Chl_{int}, mg m^{-2}) values in the fjords (Table 1) during phase-2.

Vertical distribution of in situ measured Chl-*a* and Pheo coexisted in the water column and yielded significant positive relationship between them (Fig. 7a) for Kongsfjorden ($R^2 = 0.72$, $n = 35$, $p < 0.01$) and Krossfjorden ($R^2 = 0.75$, $n = 31$, $p < 0.01$). The Chl-*a*/Pheo ratio usually decreased with increase in depths (figure not shown) and varied from 0.04 to 2.56 (0.90 ± 0.72), and from 0.08 to 5.99

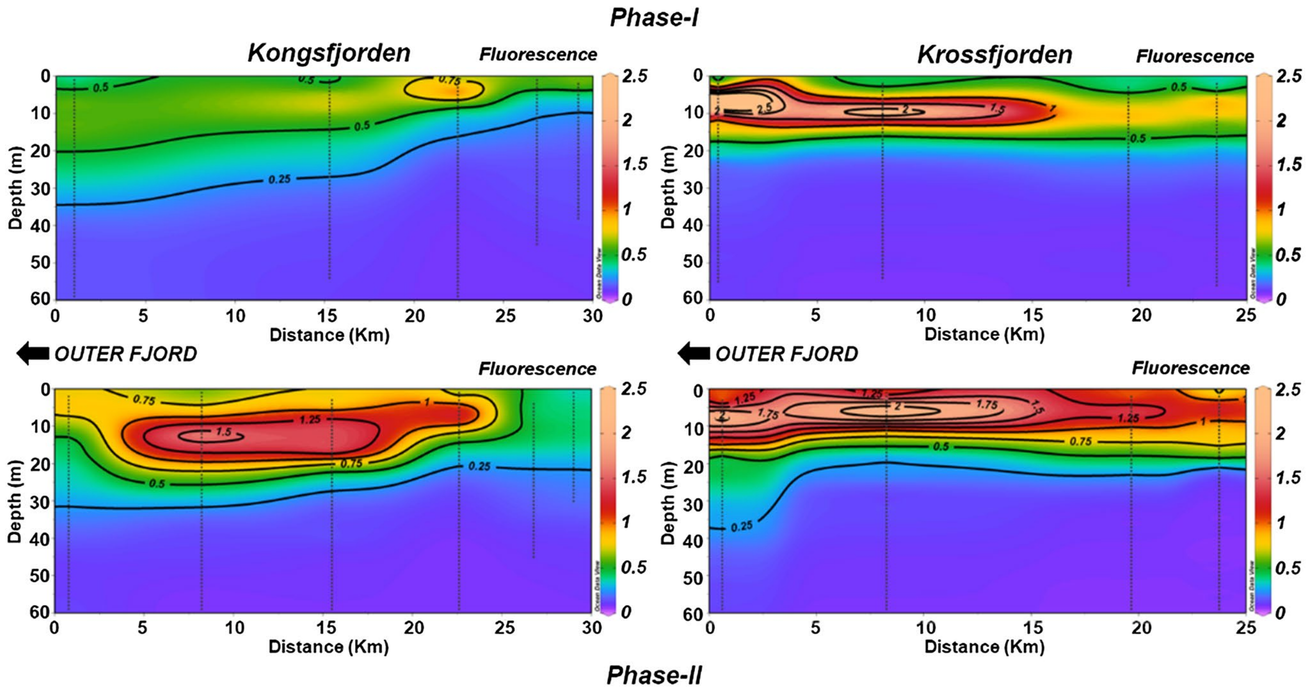

Fig. 6 Vertical distribution of chlorophyll fluorescence measured by hyperspectral radiometer equipped with ECO triplet in the Kongsfjorden (left panels) and Krossfjorden (right panels) during both the sampling phases

(1.67 ± 1.49) in Kongsfjorden and Krossfjorden, respectively. Higher average Chl-*a*/Pheo in Kongsfjorden was indicative of stronger grazing pressure and/or cell senescence under reduced growth environments (Welschmeyer and Lorenzen 1985) compared to Krossfjorden. Calleja et al. (2017) observed high contributions of Pheo relative to the Chl-*a* during summer attributable to zooplankton grazing (Lalande et al. 2016) and senescence of phytoplankton cell in unfavorable nutrient conditions. The observed nutrient limitation in both fjords corroborates the underlying fact for Pheo formation. Decrease in air temperature and solar insolation, compared to the preceding month, during summer (August) was associated with higher sub-glacial runoff from the inner tidewater glaciers, causing low salinity and high turbidity in surface waters, leading to decrease in underwater light availability and increased osmotic stress, thereby considerably reducing Chl-*a* (Calleja et al. 2017) as evidenced by very low Chl-*a* fluorescence in the inner fjords (Fig. 6).

Phaeopigments and possible implication of microzooplankton grazing

Chlorophyll and Pheo are known to be the direct products of phytoplankton growth and zooplankton grazing, respectively. Moreover, the stoichiometry between Chl-*a* and Pheo (Chl-*a*/Pheo ratio) has been used to indicate herbivore grazing, and Pheo is usually considered as an indicator for herbivore grazing (Shuman and Lorenzen 1975). On this basis, this study used the parameters that are measured in situ in the field to investigate the relative role of macro- and microzooplankton as potential grazers in the study area. It is well known that photo-degradation, which decreases exponentially with depth, is largely responsible for disappearance of Pheo in the presence of light (i.e., Pheo would be removed at an accelerated rate near the surface (well-lit zone)), resulting in decreased Chl-*a*/Pheo ratio with depth (Welschmeyer 1994). Results from this study showed typically higher Chl-*a*/Pheo at the surface, where PAR was also highest, and decreased with increase in depth showing the lowest Chl-*a*/Pheo ratio at deeper depths. Furthermore, the significant positive relationship between log-transformed Pheo and PAR (Fig. 7b, c) showed higher concentrations of Pheo in the higher PAR region (upper layers). From these observations, it can be inferred that microzooplankton grazing was prevalent in the study area. Since the Pheo generated by macrozooplankton grazing quickly leaves the euphotic zone in the form of fecal pellets (heavier, fast sinking rate), it contributes less to the Pheo measured by conventional sampling (Niskin) bottles technique. Conversely, microzooplankton grazing would result in an accumulation of fecal debris (lighter, negligible sinking rate) contributing significantly to the suspended Pheo in the water column (Welschmeyer and Lorenzen 1985), as observed in this study. Samples collected by other researchers during summer indicated the dominance of microzooplankton (Asha Devi et al. Personal Communication) in both fjords. Prevalence

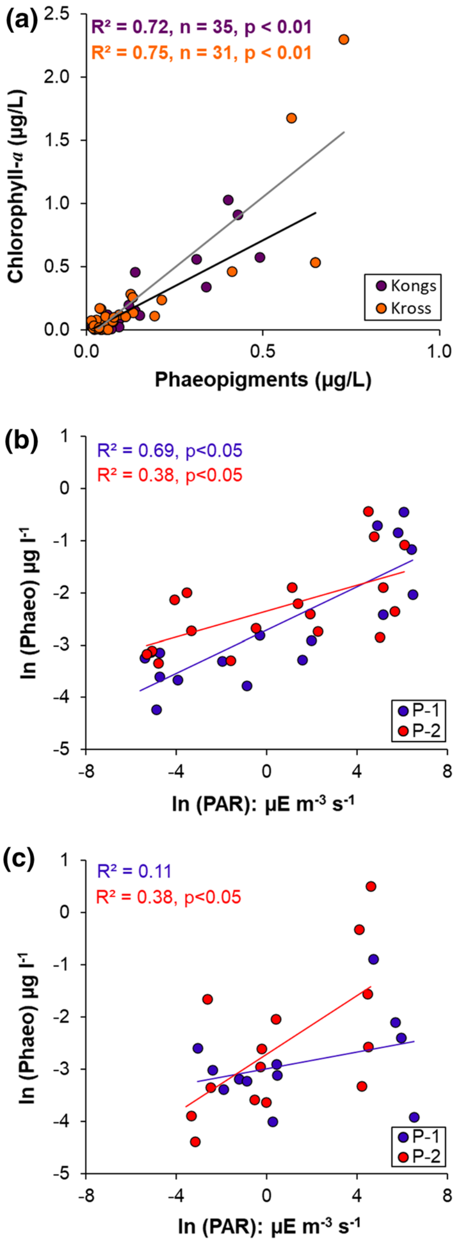

Fig. 7 (**a**) Relationship between fluorometrically measured chlorophyll-*a* and phaeopigments. Linear relationship between log-transformed phaeopigments and PAR in the (**b**) Kongsfjorden and (**c**) Krossfjorden. P-1: phase-1, P-2: phase-2

of zooplankton grazing in the light-limited inner (Eilertsen et al. 1989) and biomass-rich outer (Walkusz et al. 2009) Kongsfjorden has been documented earlier, with a special emphasis on microzooplankton (Feng et al. 2014) grazing and buildup of biomass by ciliates and dinoflagellates in the absence of large copepods (Levinsen and Nielsen 2002) during summer. Results from this study provide an assumption that Pheo may be used as a tag for microzooplankton grazing in these fjord ecosystems.

Phytoplankton pigments-based community structure and diversity index

Chromatographic analysis of the surface water samples by HPLC revealed the presence of 15 phytoplankton pigments during this study (Supplementary Table 1a). Disparity in the spatial distribution of pigments was observed inside the two fjords and between different sampling locations of the same fjord. The pigments concentrations were significantly less near the glacial end (KG5, KG4) and mid-fjord (KG2) stations in the Kongsfjorden and suddenly increased at the mouth and open ocean, whereas comparatively higher pigment concentrations were observed in the Krossfjorden. The very low pigments at the glacial end indicated inhibited phytoplankton growth due to turbidity and CDOM-induced light limitation (Kowalczuk et al. 2019). Unlike in the Kongsfjorden, higher pigment concentrations were noticed at the glacial end (KR4) of the Krossfjorden, which decreased in the mid-fjord (KR3, KR2) stations and then increased toward the mouth (KR1). α and β carotene were not identified in this study, whereas Chl-*a* pigments were below detectable limits at the near glacial end (KG5, KG4, and KG2). The observed dominant pigment was fucoxanthin (FUCO), which was present at all the stations in both fjords. The average contribution (%) of FUCO was 48.76% (Kongsfjorden) and 36.38% (Krossfjorden) followed by Chl c2, which contributed 21.16% and 31.90% in Kongsfjorden and Krossfjorden, respectively (Fig. 2S, supplementary material). The average contribution of Chl c3 was higher in the Kongsfjorden (12.14%) than Krossfjorden (9.76%). These three pigments (FUCO, Chl c2 + c3) are specific pigment markers for phytoplankton groups such as Bacillariophyceae, Chrysophyceae, and Pavlovophyceae (Johnsen and Sakshaug 2007; Pettersen et al. 2011) in the North Atlantic waters. Their contribution accounted for 56–95% of the total accessory pigments concentrations with nearly equal average (78%) values in both fjords.

The summer season in Kongsfjorden is characterized by diverse phytoplankton communities such as dinoflagellates, cryptophytes, and other autotrophic/heterotrophic flagellates dominating the phytoplankton communities (Hop et al. 2002; Calleja et al. 2017; Bhaskar et al. 2020). This study categorized the phytoplankton size class based on the DP index and observed the prevalence of microplankton (such as diatoms and flagellates) in the surface waters of both fjords. Micro-sized assemblages contributed nearly 58% (KG1) to 100% (KG4) of the total phytoplankton community in Kongsfjorden. Though nanoplankton was absent in KG4 (cause not known) it was present in all other stations (Fig. 8), and their contribution ranged from 9% (KG1) to 19% (KG2), signifying relatively higher abundance in the near glacial than the outer stations. The nanoplankton contribution further decreased to 4% at the open ocean (O1)

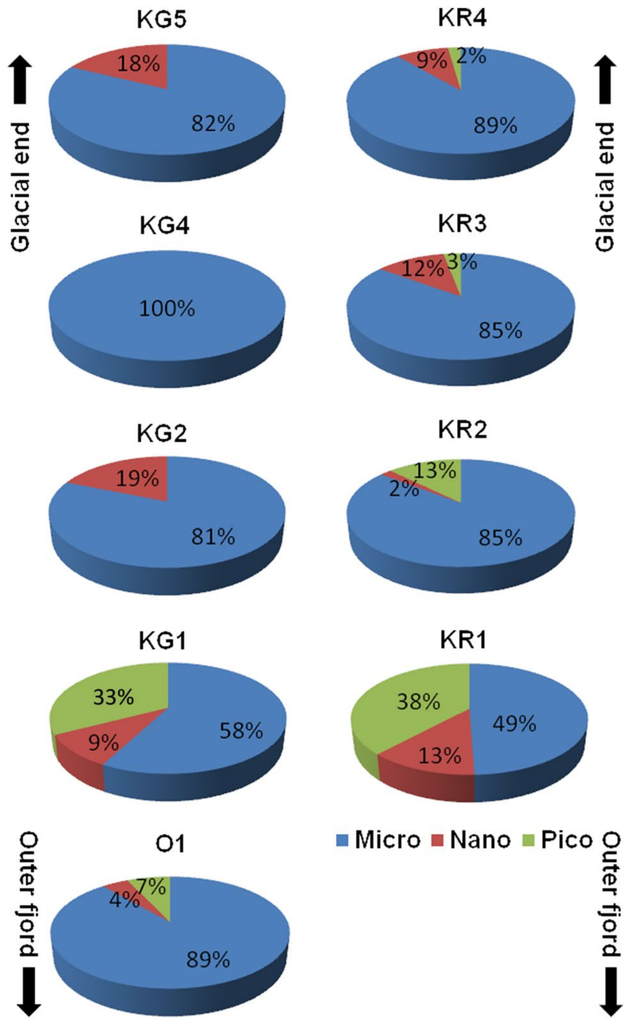

Fig. 8 Relative abundance (%) of size-fractionated phytoplankton composition in the surface waters of Kongsfjorden (left column) and Krossfjorden (right column) during phase-1 (samples not collected in phase-2)

station. Picoplankton community was conspicuously absent in the mid and near glacial (KG2, KG4, and KG5) stations, while their presence was noticed toward outer (33% at KG1 and 38% at KR1) and open ocean (7% at O1) regions, respectively. Previously, an abundance of pico- and nano-sized heterotrophs were reported during summer (July and September) in Kongsfjorden as a result of advection of these smaller plankton by the AW inflow to the fjord (Seuthe et al. 2011; Iversen and Seuthe 2011). Though cyanobacteria are often considered to be less abundant in polar waters, their increasing numbers were recorded while moving from the Arctic to AW masses in the Barents Sea (Not et al. 2005).

Though the phytoplankton community structure in Krossfjorden was different than Kongsfjorden, the dominance of microplankton was also observed in this fjord with contribution varying from 49% (KR1) to 89% (KR4) and gradually increasing from outer to inner stations (Fig. 8). Contrasting to Kongsfjorden, nano- and pico-sized individuals were recorded at all the stations of the Krossfjorden, where % contribution of nanoplankton and picoplankton prevailed over each other in the inner (KR4, KR3) and outer (KR2, KR1) stations, respectively, indicating an increase in pico-sized assemblages toward outer stations as was the case in Kongsfjorden. Prevailing very low Si/P ratio (<5) insinuated probable succession of smaller plankton over microplankton (Harrison et al. 1977; Levasseur and Therriault 1987) in this fjord, which was possibly starting during the observation period. The considerable abundance of nano- and picoplankton in Krossfjorden indicated their probable significance in ecosystem functioning as well as trophic structure in the Krossfjorden during the stratified water column in summer (Iversen and Seuthe 2011).

Published reports have shown that the absolute magnitude of phytoplankton absorption coefficients at 443 ($a_{ph}(443)$) or phytoplankton absorption slope (a_{ph}_slope) has been linked to phytoplankton taxonomy and can be used to categorize phytoplankton size class, as the microplankton (larger), nanoplankton, and picoplankton depict the largest, mid-range, and smallest a_{ph}_slope, respectively (Hirata et al. 2008; Aiken et al. 2008). To evaluate this in the study area, the a_{ph}_slope $= \delta/(|443–510|)$ was calculated, where δ is the spectral blue–green difference (i.e., $a_{ph}(443) - a_{ph}(510)$). The a_{ph}_slope varied from 0.092–0.055 m^{-1} nm^{-1} (Kongsfjorden) and from 0.076–0.012 m^{-1} nm^{-1} (Krossfjorden) and showed a decreasing trend from inner to outer fjord stations, which re-affirmed pigment analysis of this study that indicated a higher % contribution of microplankton (higher a_{ph}_slope) at the inner stations compared to outer stations, where the higher contribution of smaller plankton (lower a_{ph}_slope) was clearly seen (Fig. 8).

Pigment index, a proxy for physiological condition of the phytoplankton communities resulting from light tolerances and trophic state, was estimated to evaluate the contribution of photoprotective and photosynthetic pigments to the total pigment pool (Barlow et al. 2002; Eisner et al. 2003). Photoprotective carotenoids (PPC) (Supplementary Table 1b) were present only at outer Kongsfjorden stations (KG1, O1) and at all the stations in Krossfjorden except KR4 (innermost station) coinciding its presence in relatively clear water, where light-induced stress on phytoplankton cell often takes place (McMinn and Martin 2013). Conversely, the PPC was conspicuous by its absence in the near glacial stations characterized by turbid water. The K_d values were high (shallower Z_{eu}) in the innermost stations of Kongsfjorden, where the PPC was totally absent. Moreover, the observed average K_d value in Kongsfjorden (high) and Krossfjorden (low) confirmed that the water column was less transparent in the former than in later, which would enable higher light penetration, thereby forcing the phytoplankton to high-light acclimated condition in Krossfjorden and outer Kongsfjorden. Singh and Krishnan (2019) observed comparatively higher PPC in the sediment samples of the clearer outer stations (with deeper Z_{eu}) than in the turbid middle and inner Kongsfjorden. Considering the observed steady nutrient limitation throughout the fjords, the increase in PPC could be attributed to the response of phytoplankton to the elevated light condition in less turbid (Shibata et al. 2010; Monero et al. 2012) outer stations indicating high-light acclimation. The presence of photosynthetic carotenoids (PSC) was discerned throughout the transect in both fjords with a slightly higher percentage contribution to the pigment pool in Kongsfjorden (48.26%) than the Krossfjorden (45.23%).

The group diversity index (H') ranged from a maximum of 0.93 (KG1) to a minimum of 0.495 (KG2), implying relatively lesser diversity in the mid and inner fjord compared to outer fjord, whereas Krossfjorden displayed overall more group diversity than Kongsfjorden with relatively higher diversity toward outer stations (KR1, KR2). The group evenness index (J') was higher at outer stations in both fjords (Table 3). Surface waters of inner Krossfjorden are often relatively less turbid than inner Kongsfjorden (Piquet et al. 2010), which results in a deeper euphotic layer in Krossfjorden thereby supporting higher phytoplankton growth, abundance, and diversity in the clearer waters (Piwosz et al. 2009; Calleja et al. 2017; Singh and Krishnan 2019; Halbach et al. 2019). The observed high K_d values associated with turbidity and CDOM in this study are concurrent with previous reports and imply unfavorable condition for the growth of phytoplankton at the glacial end, especially in Kongsfjorden.

Table 3 Phytoplankton diversity index (H') and evenness (J') observed in the study area

Stations	H'	Evenness (J')
KG5	0.498	0.712
KG4	0	0
KG2	0.495	0.708
KG1	0.93	0.835
O1	0.83	0.83
KR4	0.637	0.637
KR3	0.691	0.664
KR2	0.737	0.737
KR1	0.808	0.776

Phytoplankton light absorption coefficients and package effect

The $a_{ph}(\lambda)$ is one of the major biological determinants of underwater light field in the ocean. The $a_{ph}(\lambda)$ is influenced by changes in phytoplankton species composition and physiological conditions. Estimation of $a_{ph}(\lambda)$ is an essential component of bio-optical studies and absorption-based models of phytoplankton productivity. The average $a_{ph}(\lambda)$ was distinctly different in both fjords showing comparatively lower values in Kongsfjorden than Krossfjorden during both phases (Supplementary Table 2, Fig. 9a). The inter-phase difference in average $a_{ph}(\lambda)$ in Kongsfjorden was much lower than in Krossfjorden. Phase-2 in Krossfjorden showed the highest values among the spectra. The largest difference in

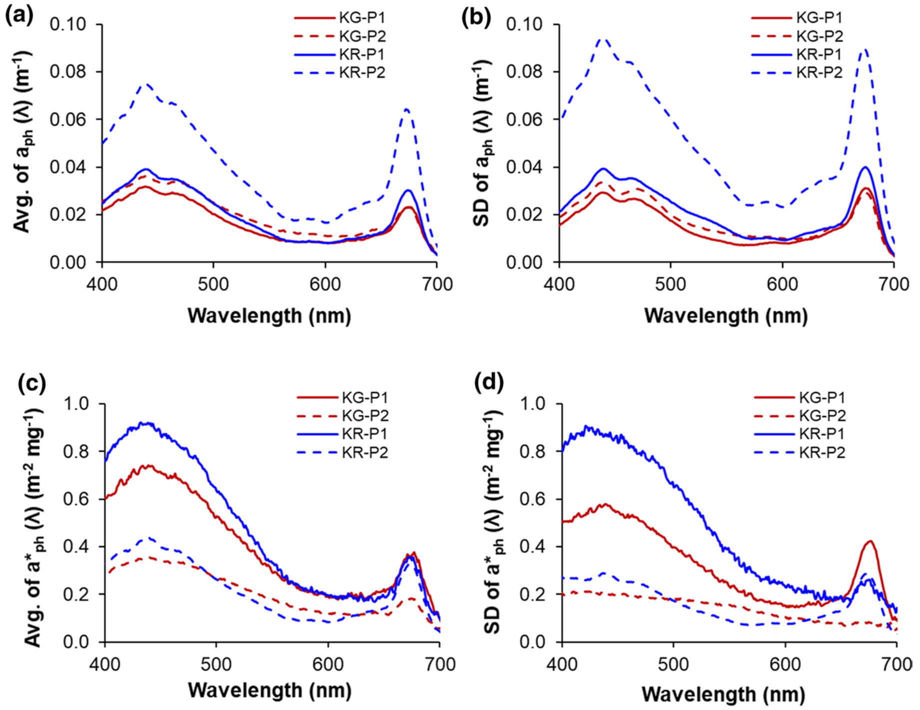

Fig. 9 (**a**) Average (Avg.) and (**b**) standard deviation (SD) of $a_{ph}(\lambda)$, and (**c**) avg. and (**d**) SD of $a^*_{ph}(\lambda)$ in the fjords. P-1: phase-1, P-2: phase-2

magnitude of $a_{ph}(\lambda)$ was observed in blue (440 nm) wavelength compared to red (675 nm). Likewise, the average Chl-*a*-specific a$_{ph}$ ($a^*_{ph}(\lambda)$) displayed dissimilarity in both magnitude and spectrum shape among the fjords and between the phases (Supplementary Table 2, Fig. 9c). The highest average $a^*_{ph}(\lambda)$ in the blue spectral region was observed in Krossfjorden phase-1 and the lowest average $a^*_{ph}(\lambda)$ in Kongsfjorden phase-2. Moreover, the Krossfjorden showed higher average $a^*_{ph}(\lambda)$ values than Kongsfjorden during both phases. The average $a_{ph}(\lambda)$ and $a^*_{ph}(\lambda)$ showed an opposite trend, i.e., higher average $a^*_{ph}(\lambda)$ was observed for the locations where lower average $a_{ph}(\lambda)$ was observed, and vice versa (Fig. 9a, c). Krossfjorden phase-1 showed the highest values among the $a^*_{ph}(\lambda)$ spectra. The standard deviation (SD) of $a_{ph}(\lambda)$ depicted high variances in Krossfjorden phase-2 (Fig. 9b), while lower variances were observed for other phases in both fjords. Relatively higher variances in $a^*_{ph}(\lambda)$ were observed for Krossfjorden and Kongsfjorden during phase-1 (Fig. 9d).

The relationships between $a_{ph}(440)$, $a_{ph}(490)$, and $a_{ph}(675)$ with Chl-*a* were different between the phases and among the fjords and showed significant positive power correlations with Chl-*a* (Fig. 10a, b, c). Large dispersion of $a_{ph}(\lambda)$ values as a function of Chl-*a* was confirmed at the blue spectral region. The scattering of data at the blue spectral region was similar (similar R^2 values) for 440 and 490 nm (Table 4), signifying that pigments (accessory) besides Chl-*a* contributed to $a_{ph}(\lambda)$ variability (Ferreira et al. 2014, 2017). This observation was reinforced by a remarkable decrease in the dispersion of $a_{ph}(675)$ as a function of Chl-*a* (note the variation in y-axes, especially in the low Chl-*a* range, Fig. 10c), as variations in this spectral range are solely attributable to Chl-*a* and the pigment package effect (Bricaud et al. 1995), which is described in the subsequent

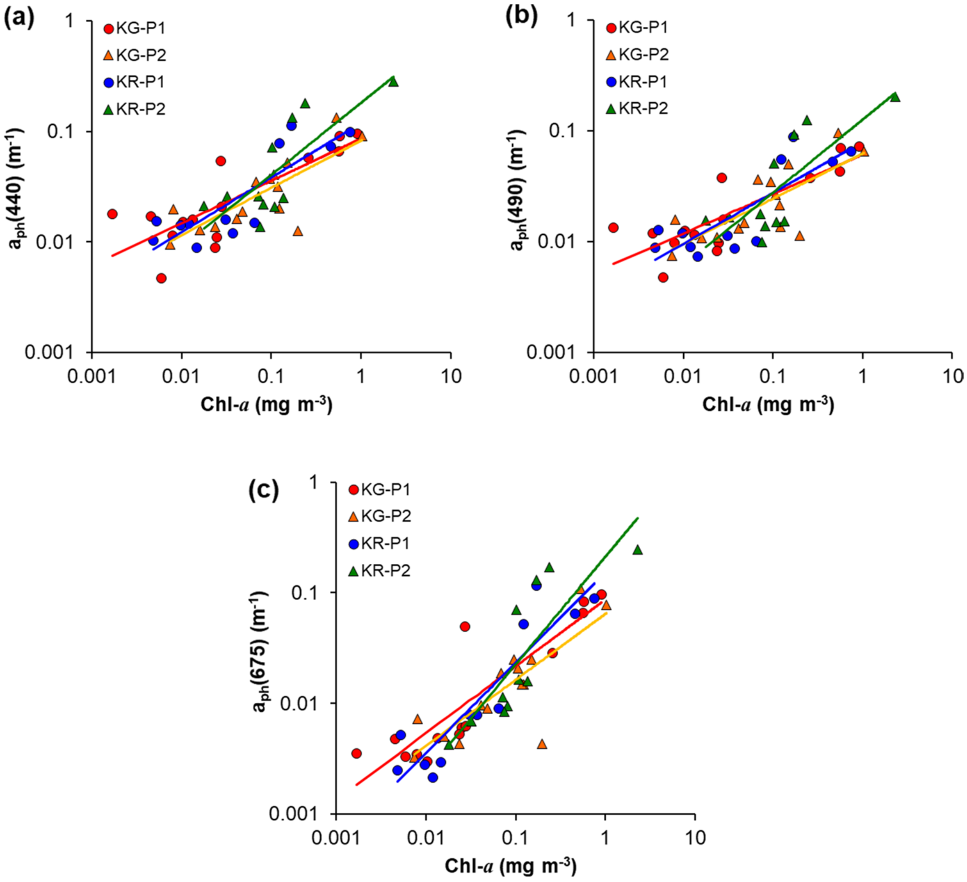

Fig. 10 Power function relationships showing phytoplankton absorption at (**a**) 440, (**b**) 490, and (**c**) 675 as a function of Chl-*a* in both fjords. The equations that describe the best fit between Chl-*a* vs. $a_{ph}(440)$, $a_{ph}(490)$, $a_{ph}(675)$ were **KG-P1:** $a_{ph}(440)=0.0862[\text{Chl-}a]^{0.3823}$ ($R^2=0.86$, $n=14$, $p<0.001$), $a_{ph}(490)=0.0611[\text{Chl-}a]^{0.3559}$ ($R^2=0.84$, $n=14$, $p<0.001$), $a_{ph}(675)=0.0868[\text{Chl-}a]^{0.6028}$ ($R^2=0.86$, $n=14$, $p<0.001$); **KG-P2:** $a_{ph}(440)=0.0824[\text{Chl-}a]^{0.4262}$ ($R^2=0.67$, $n=15$, $p<0.001$), $a_{ph}(490)=0.0626[\text{Chl-}a]^{0.4075}$ ($R^2=0.62$, $n=15$, $p<0.001$), $a_{ph}(675)=0.0644[\text{Chl-}a]^{0.5952}$ ($R^2=0.72$, $n=15$, $p<0.001$); **KR-P1:** $a_{ph}(440)=0.1189[\text{Chl-}a]^{0.4917}$ ($R^2=0.73$, $n=12$, $p<0.01$), $a_{ph}(490)=0.0797[\text{Chl-}a]^{0.46}$ ($R^2=0.60$, $n=12$, $p<0.01$), $a_{ph}(675)=0.1533[\text{Chl-}a]^{0.8167}$ ($R^2=0.57$, $n=12$, $p<0.01$); and **KR-P2:** $a_{ph}(440)=0.1809[\text{Chl-}a]^{0.6509}$ ($R^2=0.74$, $n=11$, $p<0.01$), $a_{ph}(490)=0.1265[\text{Chl-}a]^{0.6583}$ ($R^2=0.76$, $n=11$, $p<0.01$), $a_{ph}(675)=0.2113[\text{Chl-}a]^{0.9719}$ ($R^2=0.62$, $n=11$, $p<0.01$) in this study

Table 4 Coefficients of determination (R^2) of the power function relationship between $a_{ph}(440)$, $a_{ph}(490)$, $a_{ph}(675)$, $a^*_{ph}(440)$, and $a^*_{ph}(675)$ with Chl-*a* during different phases in the study area

Location-phase	*N*	$a_{ph}(440)$ R^2	$a_{ph}(490)$ R^2	$a_{ph}(675)$ R^2	$a^*_{ph}(440)$ R^2	$a^*_{ph}(675)$ R^2
KG-P1	14	*0.66	*0.70	*0.80	*0.80	*0.49
KG P2	15	*0.62	*0.57	*0.66	*0.59	0.25
KR-P1	12	*0.73	*0.67	*0.84	*0.75	0.21
KR-P2	11	*0.60	*0.59	*0.70	0.17	0

*Significant at $p < 0.01$

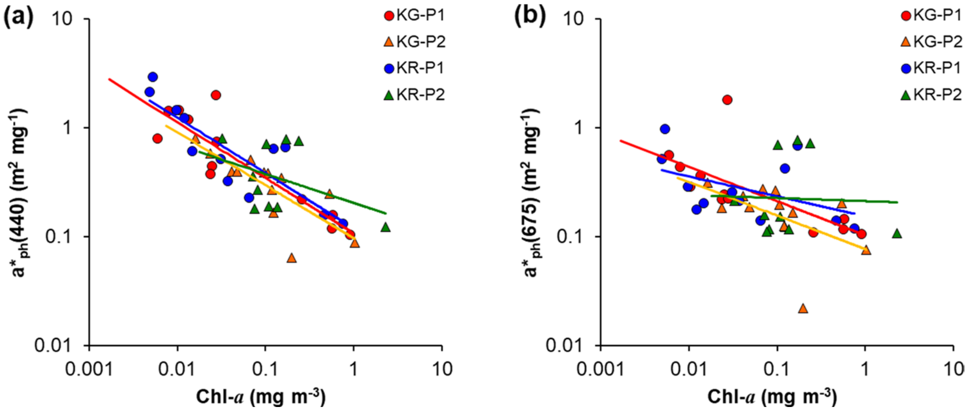

Fig. 11 Log-transformed scatter plots showing chlorophyll-specific phytoplankton absorption (a^*_{ph}) at (**a**) 440 and (**b**) 675 as a function of Chl-*a* in both fjords (P-1: phase-1, P-2: phase-2). The regression formula and the best fit parameters between Chl-*a* and $a^*_{ph}(440)$, $a^*_{ph}(675)$ were **KG-P1:** $a^*_{ph}(440) = 0.107[\text{Chl-}a]^{-0.509}$ ($R^2 = 0.43$, $n = 14$, $p < 0.01$), $a^*_{ph}(675) = 0.1025[\text{Chl-}a]^{-0.314}$ ($R^2 = 0.39$, $n = 14$); **KG-P2:** $a^*_{ph}(440) = 0.0967[\text{Chl-}a]^{-0.485}$ ($R^2 = 0.79$, $n = 14$, $p < 0.001$), $a^*_{ph}(675) = 0.0766[\text{Chl-}a]^{-0.308}$ ($R^2 = 0.38$, $n = 15$); **KR-P1:** $a^*_{ph}(440) = 0.1189[\text{Chl-}a]^{-0.508}$ ($R^2 = 0.81$, $n = 12$, $p < 0.001$), $a^*_{ph}(675) = 0.1533[\text{Chl-}a]^{-0.183}$ ($R^2 = 0.17$, $n = 12$); and **KR-P2:** $a^*_{ph}(440) = 0.2036[\text{Chl-}a]^{-0.266}$ ($R^2 = 0.08$, $n = 11$), $a^*_{ph}(675) = 0.2112[\text{Chl-}a]^{-0.029}$ ($R^2 = 0.00$, $n = 11$) in this study

paragraph. The correlations between Chl-*a* and $a_{ph}(\lambda)$ were stronger in phase-1 than in phase-2 in both fjords.

Similar to $a_{ph}(\lambda)$, the relationship between $a^*_{ph}(\lambda)$ and Chl-*a* was different between the phases and among the fjords (Fig. 11a, b). Significant negative power correlations were obtained between $a^*_{ph}(440)$ and Chl-*a* except at KR-P2 (weak correlation), whereas weak (at KG-P2, KR-P1) or no (KR-P2) correlations were observed between $a^*_{ph}(675)$ and Chl-*a* except KG-P1 (Table 4). Elevated Chl-*a* concentration is often connected to an increase in intracellular pigment concentration or cell size, which leads to lack in correlation between light-harvesting efficiency and pigment packaging originating from intracellular overlapping of the chloroplasts is termed as “package effect,” and the $a^*_{ph}(675)$ is an effective proxy for “package effect” (Bricaud et al. 1995). The coefficient $a^*_{ph}(675)$ is generally inversely correlated to Chl-*a* concentration because of the increasing package effect with Chl-*a* and an inverse co-variation between the relative abundance of accessory pigments to Chl-*a* (Bricaud et al. 1995). The observed negative power correlations of $a^*_{ph}(675)$ with Chl-*a* are indicative of the prevailing package effect (Wang et al. 2014; Alcantara et al. 2016; Chakraborty et al. 2017; Kerkar et al. 2020) in this region dominated by microplankton (in the surface layer) during the study period. To confirm this, the blue-to-red (B/R) ratio of a^*_{ph} (i.e., $a^*_{ph}(440/a^*_{ph}(675))$, which is an indicator of phytoplankton size classes (Lohrenz et al. 2003), was used. The B/R ratio of a^*_{ph} in the water column varied from 0.98 to 5.05 (avg. 2.18 ± 1.17) and 0.97 to 6.91 (avg. 2.66 ± 1.86) in KG-P1 and KR-P1, respectively (Supplementary Table 2). In principle, if the B/R is > 3.0, it denotes dominance of picoplankton (< 2 µm); if the ratio is < 2.5, the predominance of microphytoplankton (> 20 µm) is suggested (Bricaud et al. 2004; Stramski et al. 2001; Naik et al. 2010; Kerkar et al. 2021), whereas ratios between 2.5 and 3.0 indicate nanophytoplankton predominance (Aguilar-Maldonado et al. 2018). The observed average B/R ratio complemented phytoplankton pigment and a_{ph}_slope-based analysis, confirming that the surface waters of the study area were dominated by microplankton (i.e., diatoms and flagellates), which are prone to package effect, thereby resulting in reduced photosynthetic efficiency (Bricaud et al. 1995; Ferreira et al. 2017). A slightly higher average B/R ratio observed in Krossfjorden can be linked to the presence of nano- and picoplankton throughout this fjord, which are less prone to package effect, thereby having more photosynthetic efficiency. Verifying the observed relationships between Chl-*a* and a_{ph}, a^*_{ph} was not feasible due to the lack of measurements from other fjords of Svalbard with us. However, the equations proposed by us, to the best of knowledge, are the first report of its kind from these two fjords and certainly form baseline information that would facilitate future studies to use/test them while conducting bio-optical studies in the same/others fjords of Svalbard/Arctic regions.

Relationship between $a^*_{ph}(\lambda)$ with Chl-*a* has been studied in the Arctic Ocean (Matsuoka et al. 2009; Pavlov et al. 2017; Kowalczuk et al. 2019), reporting predominance of smaller plankton over larger plankton, a condition more typical of polar waters. However, the relationship has not been appreciated in these fjords, which is quite different from the open ocean condition with considerable variability in phytoplankton community structure (Hop et al. 2002). The observed relationships of the $a_{ph}(443)$ and $a_{ph}(675)$ as a function of Chl-*a* are consistent with studies undertaken in the Arctic or other higher latitudes regions (Wang et al. 2005; Matsuoka et al. 2009; Naik et al. 2010; Tripathy et al. 2014; Ferreira et al. 2017). However, the reported $a^*_{ph}(\lambda)$ values from this study are quite higher than the reported values in this region because $a^*_{ph}(\lambda)$ is derived based on the concentration of the main pigment (Chl-*a*) but since there are accessory pigments that also absorb, thereby influences the $a^*_{ph}(\lambda)$ estimates across the blue-to-red spectral range (Bricaud et al. 1995; Ferreira et al. 2017). This effect can also change within a species due to light acclimatization (Wang et al. 2005; Matsuoka et al. 2009; Kowalczuk et al. 2019). Though limited dataset did not allow us to elucidate the associated mechanism, studies have shown that algal cell adapts its photosynthetic efficiency while subjected to low-light intensity in the polar regions (Palmisano et al. 1986; Mendes et al. 2015).

Conclusion

This study demonstrates a comparative account of spatiotemporal variability in phytoplankton biomass and other optically active substances in the water column in relation to the phytoplankton community structure and photosynthetic efficiency in two high Arctic fjords during summer. Inter-phase variability of thermohaline features within the fjord implied Atlantic water inflow and mixing in these dynamic fjords, which influenced the nutrient availability. Krossfjorden was found to be less influenced by optically active substances (i.e., turbidity, CDOM) than the Kongsfjorden, where the inner fjord is tremendously affected by glacial melting-induced turbidity and CDOM. The produced CDOM was more of autochthonous (in situ) nature in Krossfjorden, whereas in Kongsfjorden, it was probably a mixture of both autochthonous and advected CDOM by Atlantic water. Higher optically active substances in Kongsfjorden resulted in the restricted euphotic zone and unfavorable conditions for phytoplankton growth. This is evidenced from observed higher phytoplankton pigment concentration and diversity index in the clearer waters of Krossfjorden than the Kongsfjorden, which is consistent with previous reports. Nitrate and silicate limitations in both fjords were conducive for the growth of non-silicious phytoplankton. The dominance of microplankton (heterotrophic flagellates and/or flagellates) was observed in the surface layer of both fjords followed by pico- and nanoplankton, which marked their appearances in relatively clearer waters of the outer fjord stations. Phytoplankton light absorption efficiency was higher in Krossfjorden than Kongsfjorden signifying its higher productivity potential. Nevertheless, the presence of microplankton in the surface layers was found to be affected by pigment packaging, which would reduce their photosynthetic efficiency. Furthermore, results from this study showed that the chlorophyll to phaeopigments ratio could probably be used as an assumption for microzooplankton grazing in these fjord ecosystems. This study reveals that despite the close geographical proximity, environmental settings in both fjords were quite dissimilar, where less optically active substances create more favorable underwater light conditions for phytoplankton photosynthesis enabling Krossfjorden to be more productive and richer in phytoplankton diversity than the Kongsfjorden. Certainly, more studies concerning phytoplankton diversity and production with respect to physicochemical and bio-optical variables are necessary in these fjords to better capture whether the differences between the fjords are periodical or permanent.

Supplementary Information The online version contains supplementary material available at https://doi.org/10.1007/s13762-021-03767-4.

Acknowledgements The authors are thankful to the Ministry of Earth Sciences (MoES), Govt. of India, for funding to conduct this study. Our sincere thanks to the Director, NCPOR, for his constant encouragement and support. Managerial support rendered by the Arctic Logistics Division of NCPOR is highly acknowledged. We thank Dr. A. Sarkar for rendering help in nutrients analysis, and Captain of *MS-Teisten* for his exemplary onboard assistance. Sincere thanks are due to the Editorial office for efficient handling of the Manuscript. We are thankful to the two anonymous reviewers for their constructive comments to improve the manuscript quality. This is NCPOR contribution number J-56/2021-22.

Author contributions SCT was involved in conceptualization, data curation, formal analysis, writing—original draft, writing—review & editing. TV helped in formal analysis, investigation. PS contributed to investigation, writing—review & editing. AUK, JTB, and SK were involved in formal analysis, methodology. BVP helped in

writing—review & editing. MG helped in formal analysis, writing—review & editing.

Funding Not Applicable.

Availability of data and material Upon request to corresponding author.

Code availability Not Applicable.

Declarations

Conflict of interest The authors declare that they have no known competing financial interests or personal relationships with other people or organizations that could have appeared to influence (bias) the work reported in this paper.

Ethical approval Not Applicable.

Consent to participate Not Applicable.

Consent for publication Not Applicable.

References

Aguilar-Maldonado J, Santamaría-del-Ángel E, González-Silvera A et al (2018) Identification of phytoplankton blooms under the index of Inherent optical properties (IOP index) in optically complex waters. Water 10(2):129. https://doi.org/10.3390/w10020129

Aiken J, Hardman-Mountford NJ, Barlow R et al (2008) Functional links between bioenergetics and bio-optical traits of phytoplankton taxonomic groups: an overarching hypothesis with applications for ocean colour remote sensing. J Plankton Res 30(2):165–181

Alcântara E, Watanabe F, Rodrigues T et al (2016) An investigation into the phytoplankton package effect on the chlorophyll-a specific absorption coefficient in Barra Bonita reservoir, Brazil. Remote Sens Lett 8:761–770. https://doi.org/10.1080/2150704X.2016.1185189

Barlow RG, Aiken J, Holligan PM et al (2002) Phytoplankton pigment and absorption characteristics along meridional transects in the Atlantic Ocean. Deep-Sea Res I 47:637–660

Beaird N, Straneo F, Jenkins W (2015) Spreading of Greenland melt waters in the ocean revealed by noble gases. Geophys Res Lett 42:7705–7713. https://doi.org/10.1002/2015GL065003

Bhaskar JT, Tripathy SC, Sabu P et al (2016) Variation of phytoplankton assemblages of Kongsfjorden in early autumn 2012: a microscopic and pigment ratio-based assessment. Environ Monit Assess 188:1–13

Bhaskar JT, Parli BV, Tripathy SC (2020) Spatial and seasonal variations of dinoflagellates and ciliates in the Kongsfjorden, Svalbard. Mar Ecol 41(3):1–12. https://doi.org/10.1111/maec.12588

Bischof K, Convey P, Duarte P et al (2019) Kongsfjorden as harbinger of the future Arctic: Knowns, unknowns and research priorities. In: Hop H, Wiencke C (eds) The ecosystem of Kongsfjorden, Svalbard. Advances in polar ecology, vol 2. Springer, Cham. https://doi.org/10.1007/978-3-319-46425-1_14

Blaszczyk M, Jania JA, Hagen JO (2009) Tidewater glaciers of Svalbard: recent changes and estimates of calving fluxes. Polish Polar Res 30:85–142

Bricaud A, Morel A, Prieur L (1981) Absorption by dissolved organic matter of the sea (yellow substance) in the UV and visible domains. Limnol Oceanogr 26:43–53

Bricaud A, Babin M, Morel A et al (1995) Variability in the chlorophyll-specific absorption coefficients of natural phytoplankton: analysis and parameterization. J Geophys Res Oceans 100(C7):13321–13332

Bricaud A, Claustre H, Ras J et al (2004) Natural variability of phytoplanktonic absorption in oceanic waters: influence of the size structure of algal populations. J Geophys Res Oceans. https://doi.org/10.1029/2004JC002419

Calleja ML, Kerhervé P, Bourgeois S et al (2017) Effects of increase glacier discharge on phytoplankton bloom dynamics and pelagic geochemistry in a high Arctic fjord. Prog Oceanogr. https://doi.org/10.1016/j.pocean.2017.07.005

Chakraborty S, Lohrenz SE, Gundersen K (2017) Photophysiological and light absorption properties of phytoplankton communities in the river-dominated margin of the northern Gulf of Mexico. J Geophys Res Oceans 122:4922–4938. https://doi.org/10.1002/2016JC012092

Cleveland JS, Weidemann AD (1993) Quantifying absorption by aquatic particles: a multiple scattering correction for glass-fiber filters. Limnol Oceanogr 38(6):1321–1327

Cohen J, Screen JA, Furtado JC et al (2014) Recent Arctic amplification and extreme mid-latitude weather. Nat Geosci 7:627–637

Cohen JH, Berge J, Moline MA et al (2015) Is ambient light during the High Arctic polar night sufficient to act as a visual cue for zooplankton? PLoS ONE 10:0126247

Cottier F, Tverberg V, Inall M et al (2005) Water mass modification in an Arctic fjord through cross-shelf exchange: the seasonal hydrography of Kongsfjorden, Svalbard. J Geophy Res 110:C12005. https://doi.org/10.1029/2004JC002757

Cottier F, Nilsen F, Inall M et al (2007) Wintertime warming of an Arctic shelf in response to large-scale atmospheric circulation. Geophys Res Lett 34:L10607. https://doi.org/10.1029/2007GL029948

Darlington E (2015) Meltwater Delivery from the Tidewater Glacier Kronebreen to Kongsfjorden, Svalbard; Insights from in situ and Remote-Sensing Analyses of sediment plumes (PhD Thesis). Loughborough University.

David DT, Krishnan KP (2017) Recent variability in the Atlantic water intrusion and water masses in Kongsfjorden, an Arctic fjord. Polar Sci 11:30–41. https://doi.org/10.1016/j.polar.2016.11.004

Eilertsen HC, Taasen JP, Weslawski JM (1989) Phytoplankton studies in the fjords of West Spitzbergen: physical environment and production in spring and summer. J Plankton Res 11:1245–1260. https://doi.org/10.1093/plankt/11.6.1245

Eisner LB, Twardowski MS, Cowles TJ et al (2003) Resolving phytoplankton photoprotective: photosynthetic carotenoid ratios on fine scales using in situ spectral absorption measurements. Limnol Oceanogr 48(2):632–646

Feng M, Zhang W, Xiao T (2014) Spatial and temporal distribution of tintinnid (Ciliophora: Tintinnida) communities in Kongsfjorden, Svalbard (Arctic), during summer. Polar Biol 37:291–296. https://doi.org/10.1007/s00300-013-1442-1

Ferrari GM (2000) The relationship between chromophoric dissolved organic matter and dissolved organic carbon in the European Atlantic coastal area and in the West Mediterranean Sea (Gulf of Lions). Mar Chem 70(4):339–357

Ferreira A, Ciotti AM, Giannini MF (2014) Variability in the light absorption coefficients of phytoplankton, non-algal particles, and colored dissolved organic matter in a subtropical bay (Brazil). Estuar Coast Shelf Sci 139:127–136

Ferreira A, Ciotti AM, Mendes CRB et al (2017) Phytoplankton light absorption and the package effect in relation to photosynthetic and photoprotective pigments in the northern tip of Antarctic Peninsula. J Geophys Res Oceans 122:7344–7363. https://doi.org/10.1002/2017JC012964

Halbach L, Vihtakari M, Duarte P et al (2019) Tidewater glaciers and bedrock characteristics control the phytoplankton growth environment in a Fjord in the Arctic. Front Mar Sci 6:254. https://doi.org/10.3389/fmars.2019.00254

Harrison PJ, Conway HL, Holmes RW et al (1977) Marine diatoms in chemostats under silicate or ammonium limitation. III. Cellular chemical composition and morphology of three diatoms. Mar Biol 43:19–31

Hegseth EN, Tverberg V (2013) Effect of Atlantic water inflow on timing of the phytoplankton spring bloom in a high Arctic fjord (Kongsfjorden, Svalbard). J Mar Syst 113–114:94–105

Hegseth EN, Assmy P, Wiktor J et al (2019) Phytoplankton seasonal dynamics in Kongsfjorden, Svalbard and the adjacent shelf. In: Hop H, Wiencke C (eds) The Ecosystem of Kongsfjorden, Svalbard, advances in Polar Ecology 2. Springer, Cambridge, pp 173–228

Hirata T, Aiken J, Hardman-Mountford NJ et al (2008) An absorption model to determine phytoplankton size classes from satellite ocean colour. Remote Sens Environ 112:3153–3159

Hodal H, Falk-Petersen S, Hop H et al (2012) Spring bloom dynamics in Kongsfjorden, Svalbard: nutrients, phytoplankton, protozoans and primary production. Polar Biol 35:191–203. https://doi.org/10.1007/s00300-011-1053-7

Hop H, Pearson TH, Hegset EN et al (2002) The marine ecosystem of Kongsfjorden, Svalbard. Polar Res 21:167–208. https://doi.org/10.1111/j.1751-8369.2002.tb00073.x

Hop H, Falk-Petersen S, Svendsen H et al (2006) Physical and biological characteristics of the pelagic system across Fram Strait to Kongsfjorden. Prog Oceanogr 71:182–231

Iversen KR, Seuthe L (2011) Seasonal microbial processes in a high-latitude fjord (Kongsfjorden, Svalbard): I. Heterotrophic bacteria, picoplankton and nanoflagellates. Polar Biol 34:731–749. https://doi.org/10.1007/s00300-010-0929-2

JGOFS (1994) Protocols for the joint global ocean flux study (JGOFS) core measurements. IOC Manual and Guides 29: 181

Johnsen G, Sakshaug E (2007) Biooptical characteristics of psii and psi in 33 species (13 pigment Groups) of marine phytoplankton, and the relevance for pulse amplitude-Modulated and fast-repetition-rate fluorometry. J Phycol 43:1236–1251. https://doi.org/10.1111/j.1529-8817.2007.00422.x

Johansen B, Tømmervik H (2013) The relationship between phytomass NDVI and vegetation communities on Svalbard. Int J Appl Earth Obs Geoinf. https://doi.org/10.1016/j.jag.2013.07.001

Kerkar AU, Tripathy SC, Minu P et al (2020) Variability in primary productivity and bio-optical properties in the Indian sector of the Southern Ocean during an austral summer. Polar Biol 43(10):1469–1492. https://doi.org/10.1007/s00300-020-02722-2

Kerkar AU, Tripathy SC, David JH et al (2021) Characterization of phytoplankton productivity and bio-optical variability of a polar marine ecosystem. Prog Oceanogr 195:102573

Kirk JTO (1994) Light and photosynthesis in aquatic ecosystems. Cambridge University Press, Cmabridge, p 509

Kowalczuk P, Sagan S, Makarewicz A et al (2019) Bio-optical properties of surface waters in the Atlantic Water inflow region off Spitsbergen (Arctic Ocean). J Geophys Res Oceans 124:1964–1987. https://doi.org/10.1029/2018JC014529

Kulk G, van de Poll WH, Buma AGJ (2018) Photophysiology of nitrate limited phytoplankton communities in Kongsfjorden, Spitsbergen. Limnol Oceanogr 63:2606–2617

Kurian S, Roy R, Repeta DJ et al (2012) Seasonal occurrence of anoxygenic photosynthesis in Tillari and Selaulim reservoirs, western India. Biogeosciences 9(7):2485–2495. https://doi.org/10.5194/bg-9-2485-2012

Lalande C, Moriceau B, Leynaert A et al (2016) Spatial and temporal variability in export fluxes of biogenic matter in Kongsfjorden. Polar Biol. https://doi.org/10.1007/s00300-016-1903-4

Levasseur ME, Therriault JC (1987) Phytoplankton biomass and nutrient dynamics in a tidally induced upwelling: the role of NO_3:SiO_4 ratio. Mar Ecol Prog Ser 39:87–97

Levinsen H, Nielsen TG (2002) The trophic role of marine pelagic ciliates and heterotrophic dinoflagellates in arctic and temperate coastal ecosystems: a cross-latitude comparison. Limnol Oceanogr 47(2):427–439

Lohrenz SE, Weidemann AD, Tuel M (2003) Phytoplankton spectral absorption as influenced by community size structure and pigment composition. J Plankt Res 25(1):35–61

Matsuoka A, Larouche P, Poulin M et al (2009) Phytoplankton community adaptation to changing light levels in the southern Beaufort Sea, Canadian Arctic. Estuar Coast Shelf Sci 82:537–546

McMinn A, Martin A (2013) Dark survival in a warming world. Proc R Soc B 280:20122909. https://doi.org/10.1098/rspb.2012.2909

Mendes CRB, Kerr R, Tavano VM et al (2015) Cross-front phytoplankton pigments and chemotaxonomic groups in the Indian sector of the Southern Ocean. Deep-Sea Res II 118:221–232. https://doi.org/10.1016/j.dsr2.2015.01.003

Mitchell BG (1990) Algorithms for determining the absorption coefficient for aquatic particulates using the quantitative filter technique. In Ocean optics X Sep 1 (Vol. 1302, pp. 137–148). International Society for Optics and Photonics

Mitchell BG, Kahru M, Wieland J et al (2002) Determination of spectral absorption coefficients of particles, dissolved material and phytoplankton for discrete water samples. In G. S. Fargion & J. L. Mueller (Eds.), Ocean Optics Protocols For Satellite Ocean Color Sensor Validation, Revision 3 (NASA Tech. Memo., vol. 2, pp. 231–257). Greenbelt, MD: National Aeronautics and Space Administration, Goddard Space Flight Center

Moreno DV, Marrero JP, Morales J et al (2012) Phytoplankton functional community structure in Argentinian continental shelf determined by HPLC pigment signatures. Estuar Coast Shelf Sci 100:72–81. https://doi.org/10.1016/j.ecss.2012.01.007

Naik P, D'Sa E, Goes JI et al (2010) Assessment of particulate absorption properties in the southeastern Bering Sea from in-situ and remote sensing data. J Appl Remote Sens 4(1):043561. https://doi.org/10.1117/1.3525572

Not F, Massana R, Latasa M et al (2005) Late summer community composition and abundance of photosynthetic picoeukaryotes in Norwegian and Barents Sea. Limnol Oceanogr 50:1677–1686

Palmisano AC, SooHoo JB, SooHoo SL et al (1986) Photoadaptation in Phaeocystis pouchetii advected beneath annual sea ice in McMurdo Sound Antarctica. J Plankton Res 8(5):891–906

Para J, Coble PG, Charriere B et al (2010) Fluorescence and absorption properties of chromophoric dissolved organic matter (CDOM) in coastal surface waters of the northwestern Mediterranean Sea, influence of the Rhone River. Biogeosciences 7:4083–4103. https://doi.org/10.5194/bg-7-4083-2010

Pavlov AK, Silyakova A, Granskog MA et al (2014) Marine CDOM accumulation during a coastal Arctic mesocosm experiment: no response to elevated pCO2 levels. J Geophys Res 119:1216–1230. https://doi.org/10.1002/2013JG002587

Pavlov AK, Taskjelle T, Kauko HM et al (2017) Altered inherent optical properties and estimates of the underwater light field during an Arctic under-ice bloom of Phaeocystis pouchetii. J Geophys Res Oceans 122:4939–4961. https://doi.org/10.1002/2016JC01247

Pavlov AK, Leu E, Hanelt D et al (2019) The underwater light climate in Kongsfjorden and its ecological implications. In: Hop H, Wiencke C (eds) The ecosystem of Kongsfjorden, Svalbard, advances in Polar Ecology 2. Springer, Cambridge, pp 137–172

Payne CM, Roesler CS (2019) Characterizing the influence of Atlantic water intrusion on water mass formation and phytoplankton distribution in Kongsfjorden Svalbard. Cont Shelf Res. https://doi.org/10.1016/j.csr.2019.104005

Pettersen R, Johnsen G, Berge J et al (2011) Phytoplankton chemotaxonomy in waters around the Svalbard archipelago reveals high amounts of Chl b and presence of gyroxanthin-diester. Polar Biol 34:627–635. https://doi.org/10.1007/s00300-010-0917-6

Pielou EC (1966) The measurement of diversity in different types of biological collections. J Theor Biol 13:131–144

Piquet AMT, Scheepens JF, Bolhuis H et al (2010) Variability of protistan and bacterial communities in two Arctic fjords (Spitsbergen). Polar Biol 33:1521–1536. https://doi.org/10.1007/s00300-010-0841-9

Piquet AMT, van de Poll WH, Visser RJW et al (2014) Springtime phytoplankton dynamics in Arctic Krossfjorden and Kongsfjorden (Spitsbergen) as a function of glacier proximity. Biogeosciences 11:2263–2279. https://doi.org/10.5194/bg-11-2263-2014

Piwosz K, Walkusz W, Hapter R et al (2009) Comparison of productivity and phytoplankton in a warm (Kongsfjorden) and a cold (Hornsund) Spitsbergen fjord in mid-summer 2002. Polar Biol 32:549–559. https://doi.org/10.1007/s00300-008-0549-2

Popova EE, Yool A, Coward AC et al (2010) Control of primary production in the Arctic by nutrients and light: insights from a high resolution ocean general circulation model. Biogeosciences 7:3569–3591. https://doi.org/10.5194/bg-7-3569-2010

Seuthe L, Iversen KR, Narcy F (2011) Microbial processes in a high-latitude fjord (Kongsfjorden, Svalbard): II. Ciliates and Dinoflagellates. Polar Biol 34:751–776. https://doi.org/10.1007/s00300-010-0930-9

Shannon C, Weaver W (1949) The mathematical theory of communication. University of Illinois Press, Urbana, IL, p 117

Shibata T, Tripathy SC, Ishizaka J (2010) Phytoplankton pigment change as a photoadaptive response to light variation caused by tidal cycle in Ariake Bay, Japan. J Oceanogr 66:831–843

Shuman FR, Lorenzen CJ (1975) Quantitative degradation of chlorophyll by a marine herbivore. Limnol Oceanogr 20(4):580–586

Singh A, Krishnan KP (2019) The spatial distribution of phytoplankton pigments in the surface sediments of the Kongsfjorden and Krossfjorden ecosystem of Svalbard, Arctic. Reg Stud Mar Sci. https://doi.org/10.1016/j.rsma.2019.100815

Stedmon CA, Markager S (2001) The optics of chromophoric dissolved organic matter (CDOM) in the Greenland Sea: an algorithm for differentiation between marine and terrestrially derived organic matter. Limnol Oceanogr 46(8):2087–2093. https://doi.org/10.4319/lo.2001.46.8.2087

Stedmon CA, Markager S, Kaas H (2000) Optical properties and signatures of Chromophoric Organic Dissolved Matter (CDOM) in Danish Coastal waters. Estuar Coast Shelf Sci 51:267–278

Stedmon CA, Amon RMW, Rinehart AJ et al (2011) The supply and characteristics of colored dissolved organic matter (CDOM) in the Arctic Ocean: Pan Arctic trends and differences. Mar Chem 124(1):108–118. https://doi.org/10.1016/j.marchem.2010.12.007

Stramska M, Stramski D, Hapter R et al (2003) Bio-optical relationships and ocean color algorithms for the north polar region of the Atlantic. J Geophys Res 108(C5):3143. https://doi.org/10.1029/2001JC001195

Stramski D, Bricaud A, Morel A (2001) Modeling the inherent optical properties of the ocean based on the detailed composition of the planktonic community. Appl Opt 40(18):2929–2945

Svendsen H, Beszczynska-Møller A, Hagen JO et al (2002) The physical environment of Kongsfjorden-Krossfjorden, an Arctic fjord system in Svalbard. Polar Res 21:133–166

Tripathy SC, Pavithran S, Sabu P et al (2014) Is primary productivity in the Indian Ocean sector of Southern Ocean affected by pigment packaging effect? Curr Sci 107(6):1019–1026

Uitz J, Claustre H, Morel A et al (2006) Vertical distribution of phytoplankton communities in open ocean: An assessment based on surface chlorophyll. J Geophys Res 111:C08005. https://doi.org/10.1029/2005JC003207

van de Poll WH, Maat D, Fischer P et al (2016) Atlantic advection driven changes in glacial meltwater: effects on phytoplankton chlorophyll-a and taxonomic composition in Kongsfjorden, Spitsbergen. Front Mar Sc 3:200. https://doi.org/10.3389/fmars.2016.00200

van de Poll WH, Kulk G, Rozema PD et al (2018) Contrasting glacial meltwater effects on post-bloom phytoplankton on temporal and spatial scales in Kongsfjorden, Spitsbergen. Elem Sci Anthropocene 6:50. https://doi.org/10.1525/elementa.307

Vihtakari M, Welcker J, Moe B et al (2018) Blacklegged kittiwakes as messengers of Atlantification in the Arctic. Sci Rep 8:1178

Walczowski W, Beszczynska-Möller A, Wieczorek P et al (2017) Oceanographic observations in the Nordic sea and fram strait in 2016 under the IO PAN long-term monitoring program AREX. Oceanologia 59:187–194. https://doi.org/10.1016/j.oceano.2016.12.003

Walkusz W, Kwasniewski S, Falk-Petersen S et al (2009) Seasonal and spatial changes in zooplankton composition in the glacially influenced Kongsfjorden, Svalbard. Polar Res 28:254–281

Wang J, Cota GF, Ruble DA (2005) Absorption and backscattering in the Beaufort and Chukchi Seas. J Geophys Res. https://doi.org/10.1029/2002JC001653

Wang SQ, Ishizaka J, Yamaguchi H et al (2014) (2014) Influence of the Changjiang River on the light absorption properties of phytoplankton from the East China Sea. Biogeosciences 11(7):1759–1773. https://doi.org/10.5194/bg-11-1759-2014

Welschmeyer NA (1994) Fluorometric analysis of chlorophyll a in the presence of chlorophyll b and pheopigments. Limnol Oceanogr 39(8):1985–1992

Welschmeyer NA, Lorenzen CJ (1985) Chlorophyll budgets: Zooplankton grazing and phytoplankton growth in a temperate fjord and the Central Pacific Gyres. Limnol Oceanogr 30(1):1–21

Woźniak B, Dera J, Ficek D et al (1999) Modelling the influence of acclimation on the absorption properties of marine phytoplankton. Oceanologia 41(2):187–210